1983

Multipole relaxation in collisions of 4(2)P potassium atoms with nitrogen and hydrogen.

Randolph William Derek Berends
University of Windsor

CANADIAN THESES ON MICROFICHE

I.S.B.N.

THESES CANADIENNES SUR MICROFICHE

National Library of Canada
Collections Development Branch

Canadian Theses on
Microfiche Service

Ottawa, Canada
K1A 0N4

Bibliothèque nationale du Canada
Direction du développement des collections

Service des thèses canadiennes
sur microfiche

NOTICE

The quality of this microfiche is heavily dependent upon the quality of the original thesis submitted for microfilming. Every effort has been made to ensure the highest quality of reproduction possible.

If pages are missing, contact the university which granted the degree.

Some pages may have indistinct print especially if the original pages were typed with a poor typewriter ribbon or if the university sent us a poor photocopy.

Previously copyrighted materials (journal articles, published tests, etc.) are not filmed.

Reproduction in full or in part of this film is governed by the Canadian Copyright Act, R.S.C. 1970, c. C-30. Please read the authorization forms which accompany this thesis.

THIS DISSERTATION
HAS BEEN MICROFILMED
EXACTLY AS RECEIVED

AVIS

La qualité de cette microfiche dépend grandement de la qualité de la thèse soumise au microfilmage. Nous avons tout fait pour assurer une qualité supérieure de reproduction.

S'il manque des pages, veuillez communiquer avec l'université qui a conféré le grade.

La qualité d'impression de certaines pages peut laisser à désirer, surtout si les pages originales ont été dactylographiées à l'aide d'un ruban usé ou si l'université nous a fait parvenir une photocopie de mauvaise qualité.

Les documents qui font déjà l'objet d'un droit d'auteur (articles de revue, examens publiés, etc.) ne sont pas microfilmés.

La reproduction, même partielle, de ce microfilm est soumise à la Loi canadienne sur le droit d'auteur, SRC 1970, c. C-30. Veuillez prendre connaissance des formules d'autorisation qui accompagnent cette thèse.

LA THÈSE A ÉTÉ
MICROFILMÉE TELLE QUE
NOUS L'AVONS REÇUE

NL-339 (r. 82/08)

Canada

6

0-315-14046-1

National Library of Canada / Bibliothèque nationale du Canada — CANADIAN THESES ON MICROFICHE / THÈSES CANADIENNES SUR MICROFICHE

61955

NAME OF AUTHOR/*NOM DE L'AUTEUR* Randolph W. D. Berends

TITLE OF THESIS/*TITRE DE LA THÈSE* Multipole relaxation in collisions of 4^2p potassium atoms with N_2 and H_2

UNIVERSITY/*UNIVERSITÉ* University of Windsor, Windsor, Ontario

DEGREE FOR WHICH THESIS WAS PRESENTED/ *GRADE POUR LEQUEL CETTE THÈSE FUT PRÉSENTÉE* M.Sc.

YEAR THIS DEGREE CONFERRED/*ANNÉE D'OBTENTION DE CE GRADE* June 1983

NAME OF SUPERVISOR/*NOM DU DIRECTEUR DE THÈSE*

Permission is hereby granted to the NATIONAL LIBRARY OF CANADA to microfilm this thesis and to lend or sell copies of the film.

The author reserves other publication rights, and neither the thesis nor extensive extracts from it may be printed or otherwise reproduced without the author's written permission.

L'autorisation est, par la présente, accordée à la BIBLIOTHÈQUE NATIONALE DU CANADA de microfilmer cette thèse et de prêter ou de vendre des exemplaires du film.

L'auteur se réserve les autres droits de publication; ni la thèse ni de longs extraits de celle-ci ne doivent être imprimés ou autrement reproduits sans l'autorisation écrite de l'auteur.

DATED/*DATÉ* May 17/83 SIGNED/*SIGNÉ* Randy Berends

PERMANENT ADDRESS/*RÉSIDENCE FIXE*

NL-91 (3-74)

MULTIPOLE RELAXATION IN COLLISIONS OF 4^2P POTASSIUM ATOMS WITH N_2 AND H_2

by

© RANDOLPH WILLIAM DEREK BERENDS

A Thesis
Submitted to the Faculty of Graduate Studies through the
Department of Physics in Partial Fulfillment
of the requirements for the Degree of
Master of Science at the
University of Windsor

Windsor, Ontario, Canada
1983

Approved by:

Dr. L. Krause (Chairman)

Dr. W. E. Baylis

Dr. D. J. McKenney

ABSTRACT

When alkali metal vapour contained in a fluorescence cell and placed in a kG magnetic field is irradiated with the corresponding monochromatic polarized resonance radiation, the atoms are preferentially excited to certain Zeeman sublevels of the resonance state, establishing a bulk multipole moment in the vapour. Collisions between the excited alkali metal atoms and other ground state atoms or molecules tend to equalize the Zeeman populations, causing multipole relaxation. The cross sections for the relaxation of the dipole, quadrupole and octupole moments may be determined from the relative intensities of the Zeeman components in the fluorescent spectrum. This thesis describes an experimental study of multipole relaxation in potassium atoms, induced by collisions with N_2 and H_2 molecules.

Circularly polarized potassium resonance radiation emitted from an electrodeless r.f. discharge lamp located in a magnetic field was passed through a narrow-band interference filter, quarter wave plate and linear polarizer, and was focused into a fluorescence cell containing K-vapour and a buffer gas, located in the field of a second electromagnet. The two magnetic fields were adjusted to permit the selective excitation of the $4^2P_{1/2\ -1/2}$ and $4^2P_{3/2\ -3/2}$ Zeeman substates. With N_2 or H_2 in the cell the other Zeeman substates became collisionally populated, causing the appearance of the corresponding components in the fluorescent spectrum. Circularly polarized fluorescence emitted parallel to the field was observed through an aperture in the pole piece of the magnet and was resolved by a piezoelectrically scanned Fabry-Perot interferometer and detected by a photomultiplier.

Measurements of the relative intensities of the Zeeman components in the fluorescent spectrum, in relation to gas pressure, yield the following multipole relaxation cross sections:

$$K\text{-}N_2(10^{-16}\,cm^2): \quad \Lambda_{1/2}^{(1)} = 59; \ \Lambda_{3/2}^{(1)} = 155; \ \Lambda_{3/2}^{(2)} = 228; \ \Lambda_{3/2}^{(3)} = 174$$

$$K\text{-}H_2(10^{-16}\,cm^2): \quad \Lambda_{1/2}^{(1)} = 46; \ \Lambda_{3/2}^{(1)} = 80; \ \Lambda_{3/2}^{(2)} = 126; \ \Lambda_{3/2}^{(3)} = 66.$$

The relatively large fine-structure mixing effects caused by these molecules were taken into account in the calculation of these cross sections.

ACKNOWLEDGEMENTS

I would like to thank Dr. L. Krause, under whose supervision this work was carried out, for his support and invaluable help in correcting the drafts of this thesis. I also wish to express my gratitude to Dr. P. Skalinski for his instruction and fellowship throughout the past year.

I would like to thank Dr. W. E. Baylis for his advice and assistance with the theoretical aspects of this work.

TABLE OF CONTENTS

LIST OF TABLES

LIST OF FIGURES

LIST OF FIGURES (cont'd)

1. INTRODUCTION

Experimental investigations of inelastic collisions between excited alkali atoms and ground-state partners, particularly noble gas atoms, have been of continuing interest for many years as these experiments provide useful information about the mechanism of collisional excitation transfer and the nature of collisional interactions. There are various processes by which an excited atom may lose all or part of its excitation energy through collisions. Collisional excitation transfer between the states of the excited atom or to the collision partner results in the emission of sensitized fluorescence of a different wavelength than that which would have resulted from the decay of the initially excited state. Quenching is the radiationless transfer of the atomic excitation energy to the various available degrees of freedom of the collision partner. Many experiments reported in recent years have been carried out to determine cross sections for fine-structure mixing and quenching in mercury and alkali metal atoms, induced in collisions with noble gas atoms and various gas molecules (Krause, 1975).

Another process which has been extensively investigated is the collisional depolarization of fluorescence. When alkali metal vapour is optically excited by polarized resonance radiation, certain Zeeman substates of the atoms may become preferentially populated, resulting in the creation of a bulk multipole moment in the vapour. (A dipole moment produced in this way is usually referred to as orientation, a quadrupole moment as alignment.) In the absence of perturbing collisions,

the fluorescence tends to be polarized in the same sense as the exciting radiation. Collisions between the excited and polarized atoms and the ground state atoms or molecules cause depolarization of the atoms and of the emitted fluorescence. The study of depolarization of atomic fluorescence in relation to buffer gas pressure provides information on the mechanism of collisional relaxation of atomic multipole moments. Depolarization experiments may be divided into two general categories, those carried out in the absence of an external magnetic field or at low fields and those carried out at strong fields. At zero field or in low magnetic fields hyperfine structure is preserved and the atomic nucleus remains coupled to the orbital electrons, while at high magnetic field strengths in the kG range, the nuclear and electronic moments of the atom become effectively decoupled (Bulos and Happer, 1971). The disorientation of sodium and potassium atoms in $^2P_{\frac{1}{2}}$ resonance states by noble gases collisions in zero field has been studied by Niewitecka et al. (1974) and Niewitecka and Krause (1975), respectively. The Hanle effect (magnetic depolarization in low fields) has been employed by Lewis, Wheeler and Wilson (1977) to study disorientation of K^2P resonance states. This technique has also been used in a modified form to determine disorientation and disalignment cross sections for Rb atoms excited to resonance states, colliding with ground state Rb atoms (Gallagher and Lewis, 1974), as well as similar cross sections for Na (Burgmans, 1979). There have been fewer experiments performed at moderate and high fields. Elbel et al. (1974) studied Na($^2P_{3/2}$) disorientation, Kamke (1975) investigated Rb disorientation and disalignment, and

Guiry and Krause (1972, 1976) determined disorientation and disalignment cross sections for collisions of Cs atoms with noble gases.

Depolarization of K ($^2P_{1/2}$ and $^2P_{3/2}$) atoms induced by collisions with noble gases at kG fields was studied by Berdowski and Krause (1968) and Berdowski, Shiner and Krause (1971). They employed a modified Zeeman scanning technique to populate selected ^2P Zeeman substates and determined the disorientation and disalignment cross sections for these gases by measuring the circular and linear depolarization of the fluorescence.

With the advent of equipment capable of resolving the individual Zeeman components in the fluorescent spectrum, it became possible to measure the cross sections for relaxation of the octupole as well as of the already measurable dipole and quadrupole moments. Baylis (1979) developed a density matrix treatment describing these collisional depolarization processes, which was based on earlier work by Fano (1957), Omont (1965), and Dyakonov and Perel (1965). Baylis' (1979) treatment allows the multipole relaxation cross sections to be obtained from the analysis of the resolved Zeeman fluorescent spectrum emitted from the excited and polarized atoms. Experiments employing Zeeman fluorescence spectroscopy to determine the multipole relaxation cross sections for collisions of K with noble gas atoms have been carried out by Boggy and Franz (1982) and by Skalinski and Krause (1982).

The interaction of excited and polarized K atoms with molecules, which forms the subject of this thesis, is more complex than collisions involving noble gases, because of the larger number of degrees of freedom available to the collision system. The resonance fine-structure mixing cross sections for collisions of potassium atoms with molecules

are larger than those for noble gases (Ciurylo and Krause, 1982, 1983). Accordingly, the density matrix treatment has been extended to include fine-structure mixing effects as well as the relaxation of the multipole moments (Baylis, 1983). The results of a recent experiment by Sieradzan and Franz (1982) indicated that the $^2P_{1/2}$ disorientation cross section for Rb in collisions with N_2 was considerably larger than the corresponding cross section for Rb-noble gas collisions. It thus seemed that the depolarization of the excited K atoms by N_2 and H_2 collisions should present an interesting and worthwhile problem for an experimental study.

This thesis describes an experiment in which the multipole relaxation and decay cross sections for the interaction of K ($^2P_{1/2}$ and $^2P_{3/2}$) atoms with N_2 and H_2 molecules were determined. The multipole moments in the vapour-gas mixture were created by selectively populating the $4^2P_{1/2}$ $_{-1/2}$ and $4^2P_{3/2}$ $_{-3/2}$ Zeeman substates of potassium by a modified Zeeman scanning technique (Berdowski and Krause, 1968). The resulting fluorescence was resolved by a scanning Fabry-Perot interferometer. Measurements of relative intensities of the fluorescent Zeeman components yielded the cross sections for collisional relaxation and decay of the dipole, quadrupole, and octupole moments.

II. THEORETICAL

Application of Density Matrix Formalism to Collisional Decay of Multipole Moments

When a potassium atom, excited to one of the 4^2P Zeeman substates, collides with a buffer gas molecule, it may be transferred to another Zeeman substate. Molecules such as N_2 and H_2 would be expected to induce transfer not only among the Zeeman substates of the $4^2P_{\frac{1}{2}}$ or $4^2P_{3/2}$ fine structure states, but also between the Zeeman substates of the $^2P_{\frac{1}{2}}$ and those of the $^2P_{3/2}$ fine structure states. The collisional process may be described by the following expressions:

$$K(4^2P_{\frac{1}{2}\ -\frac{1}{2}}) + X \rightarrow K(4^2P_{J,m}) + X + \Delta E \ , \qquad (1)$$

$$K(4^2P_{3/2\ -3/2}) + X \rightarrow K(4^2P_{J',m'}) + X + \Delta E \ , \qquad (2)$$

where X is a buffer gas molecule. When $J,J' = \frac{1}{2}$, $m,m' = \pm\frac{1}{2}$; when $J,J' = 3/2$, $m,m' = \pm 3/2$ or $\pm\frac{1}{2}$. There are altogether six Zeeman substates available to the atoms within the $^2P_{\frac{1}{2}}$, $^2P_{3/2}$ potassium doublet.

The population vector $\vec{N}$ describing the population density of the potassium atoms in these Zeeman substates must accordingly be a six-dimensional vector. The time-evolution of the population density vector $\vec{N}$ may be described using density matrix formalism (Baylis, 1979)

$$\dot{\vec{N}} = \frac{d\vec{N}}{dt} = \vec{S} - \hat{\Gamma}\,\vec{N} - \hat{\gamma}\,\vec{N} \ , \qquad (3)$$

where $\vec{S}$ represents the rate at which the Zeeman states are being optically excited, $\hat{\Gamma}$ is the matrix describing the spontaneous decay rate of

the excited state to the ground state and $\hat{\gamma}$ is the matrix describing the rate of collisional relaxation between all possible Zeeman substates. Continuous optical excitation results in a steady-state condition characterized by the rates of spontaneous decay, collisional transfer and optical excitation, and is described by

$$\vec{S} - \hat{\Gamma}\vec{N} - \hat{\gamma}\vec{N} = 0 \ . \tag{4}$$

In order to describe the population density vector $\vec{N}$ in terms of multipole densities, $\vec{N}$ must be expressed in terms of the spherical basis vectors directly related to these multipole densities. The vectors describing this six-dimensional system are obtained by defining

$$\hat{T}^T_{1L} = (\hat{u}^T_L, 0) \qquad L = 0,1 \tag{5}$$

$$\hat{T}^T_{2L'} = (0, \hat{v}^T_{L'}) \qquad L' = 0,1,2,3 \tag{6}$$

where $\hat{u}^T_L$ and $\hat{v}^T_{L'}$ are the 2-dimensional and 4-dimensional spherical basis vectors respectively (Baylis, 1983).

$$\hat{u}^T_0 = \frac{1}{\sqrt{2}}(1,1) \tag{7}$$

$$\hat{u}^T_1 = \frac{1}{\sqrt{2}}(1,-1) \tag{8}$$

$$\hat{v}^T_0 = \frac{1}{2}(1,1,1,1) \tag{9}$$

$$\hat{v}^T_1 = \frac{1}{2\sqrt{5}}(3,1,-1,-3) \tag{10}$$

$$\hat{v}^T_2 = \frac{1}{2}(1,-1,-1,1) \tag{11}$$

$$\hat{v}^T_3 = \frac{1}{2\sqrt{5}}(1,-3,3,-1) \tag{12}$$

The quantities $\vec{N}$, $\vec{S}$, $\hat{\Gamma}$ and $\hat{\gamma}$ can be expressed in a manner based on the statistical weights of the $^2P_{1/2}$ and $^2P_{3/2}$ states.

$$\vec{N} = \begin{pmatrix} \vec{N}_1 \\ \vec{N}_2 \end{pmatrix} \quad (13) \qquad \vec{N}_1 = \begin{pmatrix} N_{1/2\,1/2} \\ N_{1/2\,-1/2} \end{pmatrix} \quad (14) \qquad \vec{N}_2 = \begin{pmatrix} N_{3/2\,3/2} \\ N_{3/2\,1/2} \\ N_{3/2\,-1/2} \\ N_{3/2\,-3/2} \end{pmatrix} \quad (15)$$

$$\vec{S} = \begin{pmatrix} \vec{S}_1 \\ \vec{S}_2 \end{pmatrix} \quad (16) \qquad \vec{S}_1 = \begin{pmatrix} S_{1/2\,1/2} \\ S_{1/2\,-1/2} \end{pmatrix} \quad (17) \qquad \vec{S}_2 = \begin{pmatrix} S_{3/2\,3/2} \\ S_{3/2\,1/2} \\ S_{3/2\,-1/2} \\ S_{3/2\,-3/2} \end{pmatrix} \quad (18)$$

$$\hat{\Gamma} = \begin{pmatrix} \tau_1^{-1}\,\underset{\sim}{1}_1 & 0 \\ 0 & \tau_2^{-1}\,\underset{\sim}{1}_2 \end{pmatrix} \quad (19)$$

$$\hat{\gamma} = \begin{pmatrix} \hat{\gamma}_{11} & \hat{\gamma}_{12} \\ \hat{\gamma}_{21} & \hat{\gamma}_{22} \end{pmatrix} \quad (20)$$

$\underset{\sim}{1}_1$ is the two-dimensional identity matrix, $\underset{\sim}{1}_2$ is the four-dimensional identity matrix and 0 represents the appropriate dimensioned null matrix. τ is the average lifetime of the 4^2P state ($\tau = 2.77 \times 10^{-8}$ s, Copley and Krause, 1969). In the absence of radiation trapping $\tau = \tau_1(4^2P_{1/2}) = \tau_2(4^2P_{3/2})$, but when radiation is imprisoned by the vapour, $\tau_1 \neq \tau_2$. The $\hat{\gamma}_{ij}$ components of $\hat{\gamma}$ are (2i)x(2j) dimensional matrices. The individual elements of the $\hat{\gamma}_{ij}$ matrices are related to Z (J,m → J',m'), the rates of collisional transfer between the various Zeeman substates.

$$Z(J,m \to J',m') = NvQ(J,m \to J',m') \tag{21}$$

where N is the buffer gas number density,

$$v = \sqrt{\frac{8kT}{\pi\mu}} \tag{22}$$

is the average relative speed of the colliding partners and μ is their reduced mass. The cross section Q is the thermally averaged cross section for the transfer $(Jm \to J'm')$. Since the Zeeman splitting in each fine structure state is much smaller than kT and the collisions are isotropic (spherically symmetrical), the cross sections within each fine structure state obey the relation

$$Q(J,m \to J,m') = Q(J,-m \to J,-m') \ . \tag{23}$$

The substitution of eqs. (13), (16), (19) and (20) into eq. (4) leads to

$$\begin{pmatrix} \tau_1^{-1}\,\underset{\sim}{1}_1 + \hat{\Upsilon}_{11} & \hat{\Upsilon}_{12} \\ \hat{\Upsilon}_{21} & \tau_2^{-1}\,\underset{\sim}{1}_2 + \hat{\Upsilon}_{22} \end{pmatrix} \begin{pmatrix} \vec{N}_1 \\ \vec{N}_2 \end{pmatrix} = \begin{pmatrix} \vec{S}_1 \\ \vec{S}_2 \end{pmatrix} \tag{24}$$

The vectors $\vec{N}$ and $\vec{S}$ are now expressed in terms of the spherical basis vectors of eqs. (5) and (6).

$$\vec{N} = \begin{pmatrix} \vec{N}_1 \\ \vec{N}_2 \end{pmatrix} = \sum_{L=0}^{1} \begin{pmatrix} n_1^{(L)} \hat{u}_L \\ 0 \end{pmatrix} + \sum_{L=0}^{3} \begin{pmatrix} 0 \\ n_2^{(L)} \hat{v}_L \end{pmatrix} \tag{25}$$

where

$$n_1^{(L)} = \hat{u}_L^T \cdot \vec{N}_1 \tag{26}$$

$$n_2^{(L)} = \hat{v}_L^T \cdot \vec{N}_2 \tag{27}$$

The equations for $\vec{S}$, $s_1^{(L)}$ and $s_2^{(L)}$ follow in an identical manner. The quantities $n_1^{(L)}$ and $n_2^{(L)}$ represent the 2^L-th multipole moment density associated with $\vec{N}_1$ and $\vec{N}_2$, respectively.

$$n_1^{(0)} = \tfrac{1}{2}(N_{\frac{1}{2}\frac{1}{2}} + N_{\frac{1}{2}\,-\frac{1}{2}}) \quad \text{(occupation or monopole component of } \vec{N}_1) \tag{28}$$

$$n_1^{(1)} = \tfrac{1}{2}(N_{\frac{1}{2}\frac{1}{2}} - N_{\frac{1}{2}\,-\frac{1}{2}}) \quad \text{(orientation or dipole component of } \vec{N}_1) \tag{29}$$

$$n_2^{(0)} = \tfrac{1}{2}(N_{3/2\ 3/2} + N_{3/2\ \frac{1}{2}} + N_{3/2\ -\frac{1}{2}} + N_{3/2\ -3/2}) \tag{30}$$

(occupation component of $\vec{N}_2$)

$$n_2^{(1)} = \frac{1}{2\sqrt{5}}(3N_{3/2\ 3/2} + N_{3/2\ \frac{1}{2}} - N_{3/2\ -\frac{1}{2}} - 3N_{3/2\ -3/2}) \tag{31}$$

(orientation component of $\vec{N}_2$)

$$n_2^{(2)} = \tfrac{1}{2}(N_{3/2\ 3/2} - N_{3/2\ \frac{1}{2}} - N_{3/2\ -\frac{1}{2}} + N_{3/2\ -3/2}) \tag{32}$$

(alignment or quadrupole component of $\vec{N}_2$)

$$n_2^{(3)} = \frac{1}{2\sqrt{5}}(N_{3/2\ 3/2} - 3N_{3/2\ \frac{1}{2}} + 3N_{3/2\ -\frac{1}{2}} - N_{3/2\ -3/2}) \tag{33}$$

(octupole component of $\vec{N}_2$)

When the system is collisionally isotropic, the rotational invariance of the components of $\hat{\gamma}$, in conjunction with eq. (25), permit eq. (24) to be expressed in terms of the appropriate multipole densities (Baylis 1979).

$$\begin{pmatrix} \tau_1^{-1} + \gamma_{11}^{(L)} & \gamma_{12}^{(L)} \\ \gamma_{21}^{(L)} & \tau_2^{-1} + \gamma_{22}^{(L)} \end{pmatrix} \begin{pmatrix} n_1^{(L)} \\ n_2^{(L)} \end{pmatrix} = \begin{pmatrix} s_1^{(L)} \\ s_2^{(L)} \end{pmatrix} \tag{34}$$

The matrix elements are defined as follows:

$$\gamma_{11}^{(L)} = \hat{u}_L^T (\hat{\gamma}_{11}) \hat{u}_L \qquad L = 0,1 \tag{35}$$

$$\gamma_{22}^{(L)} = \hat{v}_L^T (\hat{\gamma}_{22}) \hat{v}_L \qquad L = 0,1,2,3 \tag{36}$$

$$\gamma_{12}^{(L)} = \hat{u}_L^T (\hat{\gamma}_{12}) \hat{v}_L \qquad L = 0,1 \tag{37}$$

$$\gamma_{21}^{(L)} = \hat{v}_L^T (\hat{\gamma}_{21}) \hat{u}_L \qquad L = 0,1 \tag{38}$$

The $\gamma_{11}^{(L)}$ and $\gamma_{22}^{(L)}$ are the multipole decay rates. The elements $\gamma_{12}^{(0)}$ and $\gamma_{21}^{(0)}$ are the fine structure excitation transfer rates for the $(^2P_{1/2} \rightarrow {}^2P_{3/2})$ and $(^2P_{3/2} \rightarrow {}^2P_{1/2})$ transitions, respectively. The elements $\gamma_{12}^{(1)}$ and $\gamma_{21}^{(1)}$ are the fine structure orientation transfer rates. All other $\gamma_{ij}^{(L)}$ terms must be zero to conserve the symmetry relationships obeyed by $\hat{\gamma}$ (Baylis, 1983).

The following equations define some of the relationships between the $\gamma_{ij}^{(L)}$ elements of eqs. (35)-(38):

$$\gamma_{11}^{(0)} = \sqrt{2} \mid \gamma_{21}^{(0)} \mid \quad (39); \qquad \gamma_{22}^{(0)} = \frac{1}{\sqrt{2}} \mid \gamma_{12}^{(0)} \mid . \tag{40}$$

The fine structure transfer rates are related as follows to the fine structure transfer cross sections $\sigma_{12}^{(0)}$ and $\sigma_{21}^{(0)}$.

$$\gamma_{12}^{(0)} = Nv\sigma_{12}^{(0)} \quad (41); \qquad \gamma_{21}^{(0)} = Nv\sigma_{21}^{(0)} \tag{42}$$

Similarly,

$$\gamma_{11}^{(0)} = Nv\sigma_{11}^{(0)} \quad (43) \qquad \gamma_{22}^{(0)} = Nv\sigma_{22}^{(0)} \tag{44}$$

Hence,

$$\sigma_{11}^{(0)} = \sqrt{2}\, \sigma_{21}^{(0)} \quad (45) \qquad \sigma_{22}^{(0)} = \frac{1}{\sqrt{2}} \sigma_{12}^{(0)} \tag{46}$$

The multipole decay cross sections $\sigma_{11}^{(1)}$ and $\sigma_{22}^{(L)}$ (L = 1,2,3) are defined by

$$\gamma_{11}^{(1)} = Nv\sigma_{11}^{(1)} \tag{47}$$

$$\gamma_{22}^{(L)} = Nv\sigma_{22}^{(L)} \tag{48}$$

The multipole relaxation rates are defined by

$$\lambda_{11}^{(1)} = Nv\Lambda_{1/2}^{(1)} \tag{49}$$

$$\lambda_{22}^{(L)} = Nv\Lambda_{3/2}^{(L)} \tag{50}$$

where $\Lambda_{1/2}^{(1)}$ and $\Lambda_{3/2}^{(L)}$ are the multipole relaxation cross sections. The various relaxation rates and cross sections defined in eqs. (43), (44), (47)-(50) are related as follows (Baylis, 1983):

$$\gamma_{11}^{(1)} = \gamma_{11}^{(0)} + \lambda_{11}^{(1)} \tag{51}$$

$$\gamma_{22}^{(L)} = \gamma_{22}^{(0)} + \lambda_{22}^{(L)} \tag{52}$$

$$\sigma_{11}^{(1)} = \sigma_{11}^{(0)} + \Lambda_{1/2}^{(1)} \tag{53}$$

$$\sigma_{22}^{(L)} = \sigma_{22}^{(0)} + \Lambda_{3/2}^{(L)} \tag{54}$$

Equations (39)-(52) are required to solve eq. (34) in terms of the multipole relaxation rates. Equation (34) yields the following solution for $\begin{pmatrix} n_1^{(L)} \\ n_2^{(L)} \end{pmatrix}$:

$$\begin{pmatrix} n_1^{(L)} \\ n_2^{(L)} \end{pmatrix} = D_L^{-1} \begin{pmatrix} \tau_2^{-1} + \gamma_{22}^{(L)} & -\gamma_{12}^{(L)} \\ -\gamma_{21}^{(L)} & \tau_1^{-1} + \gamma_{11}^{(L)} \end{pmatrix} \begin{pmatrix} s_1^{(L)} \\ s_2^{(L)} \end{pmatrix} \tag{55}$$

where $D_L = [(\tau_1^{-1} + \gamma_{11}^{(L)})(\tau_2^{-1} + \gamma_{22}^{(L)}) - \gamma_{21}^{(L)}\ \gamma_{12}^{(L)}]$. (56)

The variable $K_{ab}^{LL'}$ is now defined to facilitate the manipulation of eq. (55).

$$K_{ab}^{LL'} = \frac{n_b^{(L)}}{n_b^{(L')}} \cdot \frac{s_a^{(L')}}{s_a^{(L)}} \qquad a,b = 1,2 \tag{57}$$

The solution of eq. (55) follows by considering the two experimental cases, of which one involves the optical population of the $4^2P_{1/2\ -1/2}$ state and the other the excitation of the $4^2P_{3/2\ -3/2}$ state. Equation (34) must be manipulated to obtain expressions for $n_1^{(L)}$ and $n_2^{(L)}$ for the appropriate L,L' values and optical excitation modes.

(i) When the $^2P_{1/2\ -1/2}$ state is optically excited, $\vec{S}_1 = \begin{pmatrix} 0 \\ S_{1/2\ -1/2} \end{pmatrix}$ and $s_2^{(L)} = 0$ for L = 0,1,2,3. Equations (55)-(57) then yield the following ratios:

$$K_{11}^{01} = \frac{n_1^{(0)}\ s_1^{(1)}}{n_1^{(1)}\ s_1^{(0)}} = \frac{[\tau_2^{-1} + \gamma_{22}^{(0)}]}{[\tau_2^{-1} + \gamma_{22}^{(1)}]} \cdot \frac{D_1}{D_0} \tag{58}$$

$$K_{12}^{01} = \frac{\gamma_{21}^{(0)}}{\gamma_{21}^{(1)}} \cdot \frac{D_1}{D_0} \tag{59}$$

(ii) When the $^2P_{3/2\ -3/2}$ state is optically excited, $s_1^{(L)} = 0$ L = 0,1

and $\vec{S}_2 = \begin{pmatrix} 0 \\ 0 \\ 0 \\ S_{3/2\ -3/2} \end{pmatrix}$ (60)

$$K_{21}^{01} = \frac{\gamma_{12}^{(0)}}{\gamma_{12}^{(1)}} \cdot \frac{D_1}{D_0} \qquad (60) \qquad K_{22}^{01} = \frac{(\tau_1^{-1} + \gamma_{11}^{(0)})}{(\tau_1^{-1} + \gamma_{11}^{(1)})} \cdot \frac{D_1}{D_0} \qquad (61)$$

$$K_{22}^{02} = (\tau_1^{-1} + \gamma_{11}^{(0)}) \cdot \frac{D_2 \cdot \tau_1}{D_0} \qquad (62)$$

$$K_{22}^{03} = (\tau_1^{-1} + \gamma_{11}^{(0)}) \cdot \frac{D_3 \cdot \tau_1}{D_0} \qquad (63)$$

The $K_{ab}^{LL'}$ are related to the experimentally measured intensity ratios of the components in the resolved Zeeman fluorescent spectra. The explicit forms of the $K_{ab}^{LL'}$ are derived from eq. (59) using the definition of $n_1^{(L)}$, $n_2^{(L)}$, $s_1^{(L)}$ and $s_2^{(L)}$ given in eqs. (26)-(33).

Since in this experiment only circularly polarized radiation was detected, the ratios of the Zeeman state populations $\frac{N_{Jm}}{N_{J'm'}}$ can be obtained from the measured intensity ratios using the appropriate Einstein A coefficients which describe the decay rates of the excited states by circularly polarized radiation (Mitchell and Zemansky, 1961).

The decay of the excited states occurs by both linearly polarized π light emitted perpendicularly to the magnetic field and circularly polarized light emitted parallel to the magnetic field. For the $4^2P_{\frac{1}{2}} \rightarrow 4^2S_{\frac{1}{2}}$ transition

$$A^{\pi}_{\frac{1}{2}\,\pm\frac{1}{2}} : A^{\sigma}_{\frac{1}{2}\,\pm\frac{1}{2}} = 1:2 \qquad (64)$$

where $A^{\pi}_{\frac{1}{2}\,\pm\frac{1}{2}}$ and $A^{\sigma}_{\frac{1}{2}\,\pm\frac{1}{2}}$ are the transition probabilities for the decay of the $^2P_{\frac{1}{2}\,\pm\frac{1}{2}}$ substates by emission of π and $\sigma^{\pm}$ polarized light, respectively.

For the $4^2P_{3/2} \rightarrow 4^2S_{1/2}$ transition

$$A^{\sigma}_{3/2\ \pm 3/2} : A^{\sigma}_{3/2\ \pm 1/2} : A^{\pi}_{3/2\ \pm 1/2} = 3:1:2 \tag{65}$$

where $A^{\sigma}_{3/2\ \pm 1/2}$ and $A^{\pi}_{3/2\ \pm 1/2}$ are the transition probabilities for the decay of the $4^2P_{3/2\ \pm 1/2}$ substate by the emission of $\sigma^{\pm}$ and π polarized radiation, respectively, and $A^{\sigma}_{3/2\ \pm 3/2}$ is the transition probability for the decay of the $4^2P_{3/2\ \pm 3/2}$ substates by $\sigma^{\pm}$ polarized radiation. When only the $\sigma^{\pm}$ components emitted parallel to the magnetic field are detected, the above relationships may be summarized by the following expression, relating the actual population ratios to the measured intensity ratios.

$$\frac{N_{Jm}}{N_{J'm'}} = \frac{I_{Jm}}{I_{J'm'}} \cdot \frac{A^{\sigma}_{J'm'}}{A^{\sigma}_{Jm}} \tag{66}$$

where $A^{\sigma}_{3/2\ \pm 3/2} : A^{\sigma}_{3/2\ \pm 1/2} : A^{\sigma}_{1/2\ \pm 1/2} = 3:1:2.$ (67)

The explicit forms of the $K^{LL'}_{ab}$ values are:

$$K^{01}_{11} = \frac{\left(1 + \frac{I_{1/2\,1/2}}{I_{1/2\ -1/2}}\right)}{\left(1 - \frac{I_{1/2\,1/2}}{I_{1/2\ -1/2}}\right)} \tag{68}$$

$$K^{01}_{22} = \left(\frac{k}{-\frac{I_{3/2\ 3/2}}{I_{3/2\ -3/2}} - \frac{I_{3/2\ 1/2}}{I_{3/2\ -3/2}} + \frac{I_{3/2\ -1/2}}{I_{3/2\ -3/2}} + 1}\right) \tag{69}$$

$$K_{22}^{02} = \left(\frac{I_{3/2\ 3/2}}{I_{3/2\ -3/2}} - 3\,\frac{I_{3/2\ 1/2}}{I_{3/2\ -3/2}} - 3\,\frac{I_{3/2\ -1/2}}{I_{3/2\ -3/2}} + 1 \right)^{k} \tag{70}$$

$$K_{22}^{03} = \left(-\frac{I_{3/2\ 3/2}}{I_{3/2\ -3/2}} + 9\,\frac{I_{3/2\ 1/2}}{I_{3/2\ -3/2}} - 9\,\frac{I_{3/2\ -1/2}}{I_{3/2\ -3/2}} + 1 \right)^{k} \tag{71}$$

$$\text{where } k = \left(\frac{I_{3/2\ 3/2}}{I_{3/2\ -3/2}} + 3\,\frac{I_{3/2\ 1/2}}{I_{3/2\ -3/2}} + 3\,\frac{I_{3/2\ -1/2}}{I_{3/2\ -3/2}} + 1 \right). \tag{72}$$

The explicit forms of the D_L values ($L = 0,1,2,3$) given by eq. (56) are now listed.

$$D_0 = [(\tau_1^{-1} + \gamma_{11}^{(0)})(\tau_2^{-1} + \gamma_{22}^{(0)}) - \gamma_{21}^{(0)}\,\gamma_{12}^{(0)}] \tag{73}$$

$$D_1 = [(\tau_1^{-1} + \gamma_{11}^{(1)})(\tau_2^{-1} + \gamma_{22}^{(1)}) - \gamma_{21}^{(1)}\,\gamma_{12}^{(1)}] \tag{74}$$

$$D_2 = (\tau_1^{-1})(\tau_2^{-1} + \gamma_{22}^{(2)}) \tag{75}$$

$$D_3 = (\tau_1^{-1})(\tau_2^{-1} + \gamma_{22}^{(3)}) \tag{76}$$

The quantities $\gamma_{21}^{(0)}$, $\gamma_{12}^{(0)}$ and $\gamma_{11}^{(0)}$, $\gamma_{22}^{(0)}$ are assumed known since the fine-structure transfer cross sections $\sigma_{12}^{(0)}$ and $\sigma_{21}^{(0)}$ have been determined (Ciurylo and Krause, 1982, 1983) in zero field and at very low pressures. Equations (62) and (63) may be solved directly for $\gamma_{22}^{(2)}$ and $\gamma_{22}^{(3)}$ using these values of $\sigma_{12}^{(0)}$ and $\sigma_{21}^{(0)}$. However, eqs. (58)-(61) are coupled because of the orientation transfer rate product $\gamma_{12}^{(1)}\,\gamma_{21}^{(1)}$ contained in eq. (74). An estimate of this product can be obtained from

the experimental data assuming single collision conditions, which require the collision rate to be much smaller than the reciprocal lifetime of the excited state. Under this condition the transfer cross section between Zeeman states becomes (Skalinski, 1982):

$$Q(Jm \rightarrow J'm') = \frac{1}{Nv\tau'} \frac{N_{J'm'}}{N_{Jm}} \qquad (77)$$

The fine-structure orientation transfer rates are

$$\gamma_{12}^{(1)} = Nv\sigma_{12}^{(1)} \quad \text{and} \quad \gamma_{21}^{(1)} = Nv\sigma_{21}^{(1)} \qquad (78)$$

where $\sigma_{12}^{(1)}$ and $\sigma_{21}^{(1)}$ are the fine-structure orientation transfer cross sections. These cross sections are the sums of the appropriate elements of the individual $\hat{\gamma}_{12}$ and $\hat{\gamma}_{21}$ matrices (Baylis, 1979, eq. 83).

$$\sigma_{12}^{(1)} = \sqrt{10}\,(Q(\tfrac{1}{2}\ -\tfrac{1}{2} \rightarrow 3/2\ -\tfrac{1}{2}) - Q(\tfrac{1}{2}\ -\tfrac{1}{2} \rightarrow 3/2\ \tfrac{1}{2})) \qquad (79)$$

$$\sigma_{12}^{(1)} = \frac{\sqrt{10}}{3}\,(Q(\tfrac{1}{2}\ -\tfrac{1}{2} \rightarrow 3/2\ -3/2) - Q(\tfrac{1}{2}\ -\tfrac{1}{2} \rightarrow 3/2\ 3/2)) \qquad (80)$$

$$\sigma_{21}^{(1)} = \frac{\sqrt{10}}{3}\,(Q(3/2\ -3/2 \rightarrow \tfrac{1}{2}\ -\tfrac{1}{2}) - Q(3/2\ -3/2 \rightarrow \tfrac{1}{2}\ \tfrac{1}{2})) \qquad (81)$$

A value for $\sigma_{12}^{(1)}$ was obtained by averaging eqs. (79) and (80). It turns out that the value for the product $(\sigma_{12}^{(1)})(\sigma_{21}^{(1)})$ is zero within experimental error as shown in Table 1. Consequently, the product $\gamma_{12}^{(1)}\,\gamma_{21}^{(1)}$ may be neglected to a good approximation. Under this simplification eqs. (58) and (61)-(63) yield the multipole decay rates $\lambda_{11}^{(1)}$ and $\lambda_{22}^{(L)}$ which, in conjunction with eqs. (49)-(54) give the multipole relaxation cross sections $\Lambda_{\frac{1}{2}}^{(1)}$ and $\Lambda_{3/2}^{(L)}$:

$$\Lambda_{\frac{1}{2}}^{(1)} = \frac{1}{Nv\tau_1}\left[K_{11}^{01} - 1\right] + \left[\frac{K_{11}^{01}}{1 + Nv\tau_2(\sigma_{22}^{(0)})} - 1\right](\sigma_{11}^{(0)}) \qquad (82)$$

$$\Lambda_{3/2}^{(L)} = \frac{1}{Nv\tau_2}\left[K_{22}^{0L} - 1\right] + \left[\frac{K_{22}^{0L}}{1 + Nv\tau_1(\sigma_{11}^{(0)})} - 1\right](\sigma_{22}^{(0)}) \qquad (83)$$

Equations (82) and (83) were used to obtain the multipole relaxation cross section from the experimental measurements of the Zeeman fluorescent intensities and buffer gas pressures. It should be noted that, if fine-structure mixing is neglected, only the first term appears in eqs. (82) and (83), since the second term allows for fine-structure mixing. In the present experiment the second term introduces a correction of approximately 7% to the $\Lambda_J^{(L)}$ values, representing the contribution of fine-structure mixing to the observed multipole relaxation cross sections.

III. THE APPARATUS AND THE EXPERIMENTAL PROCEDURE

1. General Description

A schematic representation of the apparatus is shown in Fig. 1. Resonance radiation emitted from an electrodless r.f. potassium discharge lamp located in a uniform magnetic field of about 5.4 kG generated by a 12" electromagnet, was used to excite potassium vapour in a fluorescence cell placed in a second magnetic field. Coincidences between the Zeeman components of the radiation emitted from the lamp and the Zeeman transitions in the fluorescence cell were produced by varying the strength of the field surrounding the cell. This excitation method was used to selectively populate either the $4^2P_{3/2\ -3/2}$ or the $4^2P_{1/2\ -1/2}$ potassium states (Berdowski, Shiner and Krause, 1971).

The radiation emitted from the lamp parallel to the magnetic field is a mixture of right (σ^+) and left (σ^-) circularly polarized light. A prism located between the poles of the electromagnet was used to direct the light beam in a direction perpendicular to the magnetic field. It was then passed through a lens and an interference filter which separated the ($4^2P_{3/2} - 4^2S_{1/2}$) 7665 Å and ($4^2P_{1/2} - 4^2S_{1/2}$) 7699 Å components. The quarter wave plate and linear polarizer produced monochromatic σ-radiation linearly polarized along the vertical axis; this was then focused into the fluorescence cell mounted in an oven between the poles of the second electromagnet.

The resulting fluorescence was monitored perpendicularly to the exciting radiation through an aperture in the pole-piece of the

Fig. 1 Arrangement of the apparatus for Zeeman spectroscopy. L, source of exciting light; F, interference filter; P, HN-7 polaroid; M, electromagnets; F-P, interferometer; A, amplifier; RG, ramp generator - both connected to an X-Y plotter.

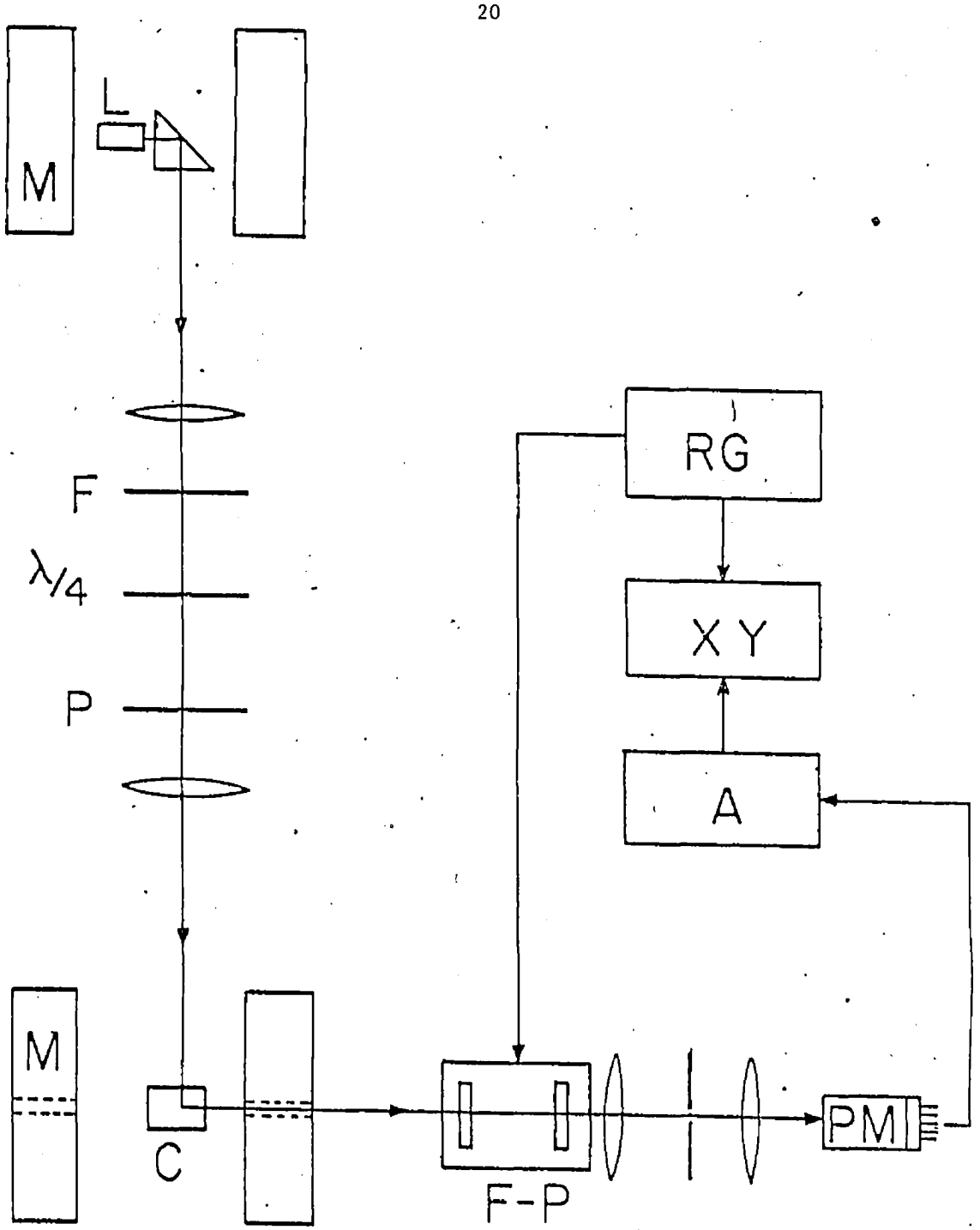

electromagnet. A lens placed in this aperture directed the fluorescence onto the mirrors of a scanning Fabry-Perot interferometer. The subsequent output radiation was brought to focus at a 1 mm pinhole and finally focused on the photocathode of a liquid nitrogen-cooled photomultiplier. The photomultiplier signal was amplified by a picoammeter and plotted on an X-Y chart recorder in relation to the plate separation of the interferometer.

2. The Spectral Lamp

The spectral lamp consisted of a pyrex cylinder 2.5 cm long and 2.5 cm in diameter fitted with plane windows and a 2.5 cm long side arm which contained approximately 1 g of potassium. The lamp also contained 0.6 torr argon to provide stability to the discharge. It was coated appropriately on the outside with a colloidal suspension of graphite to reduce the intensity of scattered light. The side arm was placed in a small electrical heating oven to allow control of the potassium vapour pressure. The main body of the lamp was placed inside an r.f. coil which was connected to a 38 MHz oscillator by coaxial cables. The operational stability of the lamp was monitored by passing part of the emitted light through an interference filter and recording the intensity with a photodiode, whose output was plotted on a strip-chart recorder. The variation in lamp intensity monitored in this manner was of the order of 1% over the usual length of an experimental scan (200 sec). The long term lamp stability was quite good, though its output intensity decreased by about 1.5% per hour of operation because of the discolouration of the pyrex envelope.

3. The Fluorescence Cell and Oven

The pyrex fluorescence cell was 6 cm long and 2.5 cm in diameter, and was fitted with two plane windows perpendicular to each other, through which exciting radiation entered and fluorescence was monitored. A side arm 4 cm long and 1.5 cm in diameter containing metallic potassium was connected to the bottom of the cell. The top of the cell was connected to the vacuum and gas filling system by a folded 2 mm capillary tube.

The buffer gas pressures, which were in the range .01 to .09 torr, were measured by an MKS Baratron capacitance gauge to provide reliable absolute gas pressure measurements. The gauge was checked against a cold-trapped McLeod gauge and the pressure variation was smaller than the scale reading uncertainty of the McLeod gauge.

The cell was located in an oven consisting of two parts, one containing the main body of the cell and the other enclosing the side arm. The temperature of the main oven was maintained by an electronic temperature controller regulated with a thermostat located in the oven. The side arm was surrounded by a copper coil through which silicon oil from an ultrathermostat was circulated. The temperature was monitored by a network of copper-constantan thermocouples referenced to $0^{\circ}C$ which were placed in the main oven and at various points along the side arm. A temperature difference of about $40^{\circ}C$ was maintained between the main oven and the side arm to prevent potassium condensation on the windows of the cell. The liquid potassium in the bottom of the side arm was estimated to have a thermal gradient of about $.25^{\circ}C$ which was less than the variation in the side arm temperature. The side arm temperature ranged between $68^{\circ}C$ and $72^{\circ}C$ over the various experimental runs.

The cell body and the inner walls of the oven were coated with colloidal graphite to reduce stray scattered light. The scattered light intensity, measured by freezing out the potassium in the cell, was found to be insignificant in comparison with the measured fluorescent intensities. The fluorescent light traversed a distance of approximately 7 mm in the vapour before reaching the exit window.

4. Electromagnets and Power Supplies

Two water-cooled Magnion Model L-128 A electromagnets with four-inch gaps and 12-inch poles were used to provide the magnetic field surrounding the lamp and the cell. In each case the homogeneity of the fields in the central region between the poles was better than 0.1%. The aperture in the pole piece of the magnet surrounding the cell facilitated the detection of fluorescence emitted parallel to the field.

The power supply for the magnet surrounding the lamp was provided by an Electronics Measurements SCR constant current power supply model 120-40. The cell magnet was powered by an EM model 120-60. The latter supply provided sufficient current to produce fields up to about 10 kG.

5. Optical Components and Photomultiplier

The light emitted by the spectral lamp was reflected by the prism and was collimated by a 25 cm focal length lens. The Spectrolab interference filters, used to separate the two resonance fine-structure components, had a rejection of less than 0.1% and a transmission of 72% in the case of the 7664.9 Å filter and 64% for the 7699 Å filter. The axes of the $\lambda/4$-plate was redetermined and oriented so that the slow and fast axes were at an angle of 45^{o} with the vertical. This

arrangement produced σ^- radiation linearly polarized parallel to the vertical axis and σ^+ radiation polarized along the horizontal axis. The axis of the linear polarizer (HN-7 polaroid) was aligned with the vertical axis to eliminate the σ^+ component.

The linearly polarized σ^- radiation was brought to focus in the fluorescence cell using a f = 7 cm lens. The fluorescence emitted parallel to the field was collimated and made incident on the mirrors of the interferometer by a f = 12.4 cm lens placed in the pole piece aperture. The light leaving the interferometer was focused at a 1 mm pinhole and the fluorescent spectrum produced by the scanning of the interferometer was focused onto the photocathode of an ITT model FW-118 photomultiplier. The latter was cooled by liquid nitrogen to reduce the dark noise to the level of 10^{-12} A, which represented approximately 0.1% of a typical signal. The photomultiplier was supplied with high voltage by a Fluke model 412-B power supply operating at 1.6 kV. The photomultiplier signal was amplified by a Keithley 417 high speed picoammeter and plotted in relation to the Fabry-Perot plate separation on a Moseley Model 20-2A XY recorder.

6. The Piezoelectrically Scanned Fabry-Perot Interferometer

A Burleigh model RC-140 Fabry-Perot interferometer placed in a thermal enclosure was used to resolve the fluorescent spectrum. The interferometer was fitted with mirrors of flatness $\lambda/200$ having a reflectivity of 96% in the spectral range 740-920 nm and a mirror spacing of .33 cm. This provided a free spectral range of 1.50 cm^{-1}.

A measure of the experimental finesse of the system was obtained by resolving the known fine-structure of the 894.346 nm cesium line

(Millman and Kusch, 1940) as shown in Fig. 2. A measurement of the separation of the interference orders and the F.W.H.H. of the narrowest peak gave an experimental finesse of about 50.

The mirrors were mounted parallel to one another in Super-Invar mountings. One mirror was fixed on the tips of three coarse alignment screws. The other mirror was mounted on three piezoelectric ceramic elements. A high-voltage ramp applied by a Burleigh Model RC-43 programmable ramp generator to the piezoelectric elements caused the latter mirror to move relative to the fixed mirror. The linearity of the piezoelectric system was better than 1% when supplied by a linear ramp voltage.

A high-voltage ramp signal with a period of 200 s, was applied to the piezoelectric element to scan the interferometer. Each spectral scan included three interference orders and, on the average, seven such traces were recorded at each of the gas pressures. This scanning rate in conjunction with the time constant of the picoammeter produced the best instrumental combination for recording an undistorted trace of the spectrum.

The parallelism of the mirrors was adjusted initially by the coarse adjustment screws. The fine alignment was accomplished by applying a bias voltage supplied by the ramp to the individual piezoelectric elements. The interference pattern generated from the light emitted by an r.f. cesium spectral lamp ($\lambda \approx 690$ nm) was used for this alignment.

7. Corrections for Radiation Trapping Effects

The potassium atoms in the fluorescent cell absorb and re-emit the fluorescent radiation, effectively increasing the radiative lifetime of

Fig. 2 The hyperfine structure spectrum of Cs 894.346 nm resonance radiation ($6^2P_{\frac{1}{2}} - 6^2S_{\frac{1}{2}}$) produced by the scanning Fabry-Perot interferometer. The first double peak arises from the $6^2P_{\frac{1}{2}}$, F = 3,4 → $6^2S_{\frac{1}{2}}$, F = 3 transitions; the second double peak corresponds to the $6^2P_{\frac{1}{2}}$, F = 3,4 → $6^2S_{\frac{1}{2}}$, F = 4 transitions. The intensities of the four components should be in the ratio 21:15:7:21 (in adequate agreement with the recording), and the hfs separation in the ground state (between peaks 1 and 2) is 0.3066 cm^{-1} (Millman and Kusch, 1940).

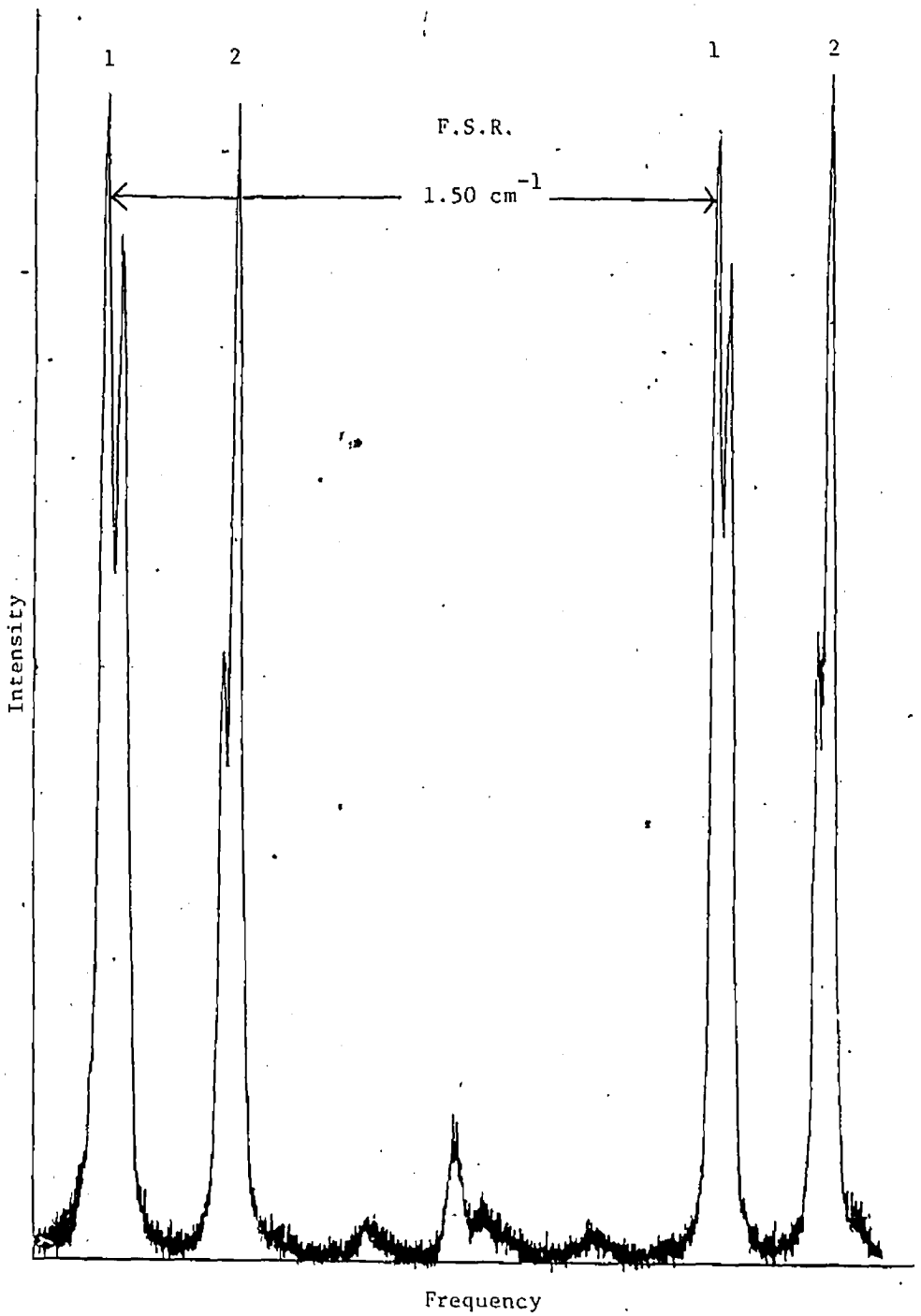

the resonance state. Because of this, the radiative lifetimes τ_1 and τ_2 which appear in eq. (19) must be corrected appropriately (Skalinski, 1982). According to the radiation diffusion treatment of Milne (Mitchell and Zemanski, 1961),

$$\tau/\tau_0 = 1 + \left(\frac{k_0 \ell}{\beta}\right)^2 . \tag{84}$$

τ is the effective (trapped) lifetime, τ_0 is the 'natural' lifetime (2.77×10^{-8} s for the 4^2P states of K), ℓ is the distance through which the radiation must diffuse, and k_0 is the absorption coefficient which was calculated assuming that the spectral lines have a Doppler shape.

$$k_0 = \frac{2}{\Delta\nu_0}\left(\frac{\ell n 2}{\pi}\right)^{\frac{1}{2}} \frac{\lambda_0^2}{8\pi} \frac{g_2}{g_1} \frac{N}{\tau_0} \tag{85}$$

$$\Delta\nu_D = \frac{2}{c}(2R\ell n 2)^{\frac{1}{2}} \nu_0 \left(\frac{T}{M}\right)^{\frac{1}{2}} \tag{86}$$

g_1 and g_2 are the statistical weights of the excited and ground states, respectively, N is the vapour density of potassium determined from temperature-vapour pressure relationships (Nesmeyanov, 1963), M is the atomic mass of K, c is the speed of light, R the ideal gas constant, and T the absolute temperature of the vapour. β is the first root of the equation

$$\tan\beta = \frac{k_0 \ell}{\beta}, \quad (0 \leq \beta \leq \pi/2) \tag{87}$$

which was solved graphically.

Because of the Zeeman splitting, all the optical depths $k_0\ell$ must be multiplied by factors appropriate to each polarized component

(Skalinski, 1982). For the $4^2P_{3/2}$ state this factor is 17/40 and for the $4^2P_{1/2}$ state it is 3/5. The effective (trapped) lifetime τ was larger than τ_0 by about 15% for the $^2P_{1/2}$ state and by about 30% for the $^2P_{3/2}$ state.

IV. RESULTS AND DISCUSSION

1. The Fluorescent Zeeman Spectra

The fluorescent Zeeman spectra were recorded as described in Chapter III, using Ar, N_2 and H_2 as buffer gases. Argon was included in the experiment to serve as a check of the experimental system against the multipole relaxation cross sections determined previously (Skalinski and Krause, 1982). The interferograms registered the intensities of the circularly polarized Zeeman components emitted parallel to the magnetic field from the potassium vapour-buffer gas mixture, subjected to either $4^2P_{\frac{1}{2}\ -\frac{1}{2}}$ or $4^2P_{3/2\ -3/2}$ excitation.

The radiative σ transitions that take place in K atoms when the $^2P_{\frac{1}{2}\ -\frac{1}{2}}$ Zeeman substate is being selectively excited, are shown in Fig. 3. Transition A arises from the decay of the optically populated state, while all other transitions arise primarily from the collisionally populated Zeeman substates, of which those belonging to the $^2P_{3/2}$ state have become populated as the result of fine-structure mixing collisions.

Because of slight imperfections in the quarter wave plate and linear polarizer, a small amount of σ^+ resonance radiation entered the cell and directly populated the corresponding Zeeman substate. The amount of σ^+ leakage was determined by scanning the spectrum in the absence of a buffer gas in the cell, as shown in Fig. 4 for the case of $^2P_{\frac{1}{2}\ -\frac{1}{2}}$ excitation. The σ^+ leakage produced a small population of the $^2P_{\frac{1}{2}\frac{1}{2}}$ Zeeman substate and resulted in the appearance of the small 'B' peak. The measured intensities of this Zeeman component recorded in the presence of a buffer gas were corrected by subtracting the proportion σ^+ leakage from this ratio.

Fig. 3 Energy level diagram of the K^2P Zeeman substates showing the σ decays to the ground state. The $4^2P_{1/2}$ $-1/2$ substate is optically populated, the other substates are populated by collisions. The spacings between energy levels are not drawn to scale and the π transitions are not shown.

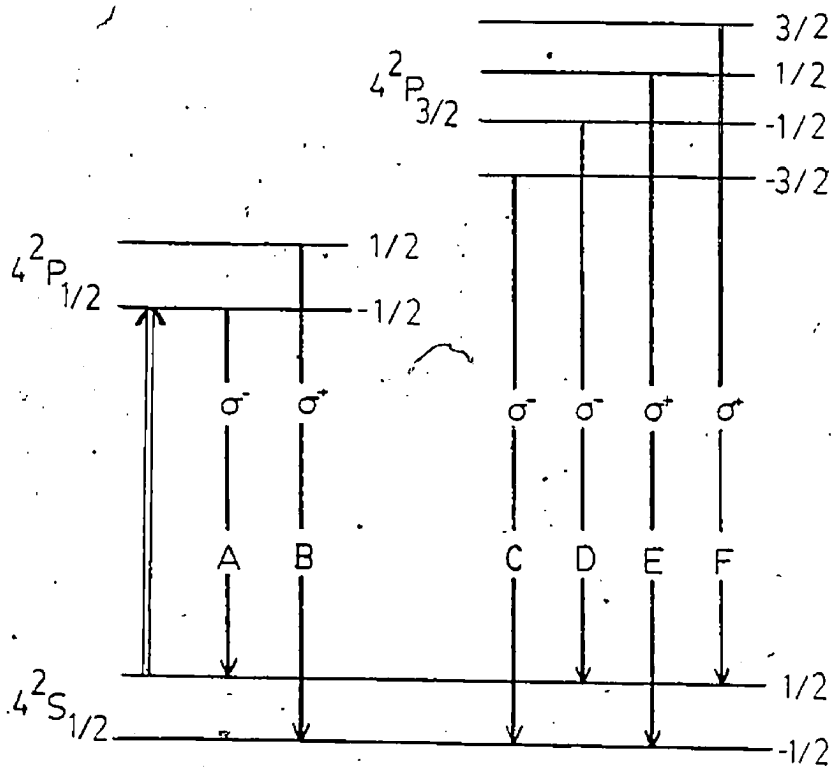

Fig. 4 A trace of the fluorescent Zeeman spectrum emitted from pure K vapour undergoing $^2P_{\frac{1}{2}} - {}^2S_{\frac{1}{2}}$ excitation. Peak B arises from the leak of σ^+ resonance radiation through the optical polarizers. The components are labelled as in Fig. 3.

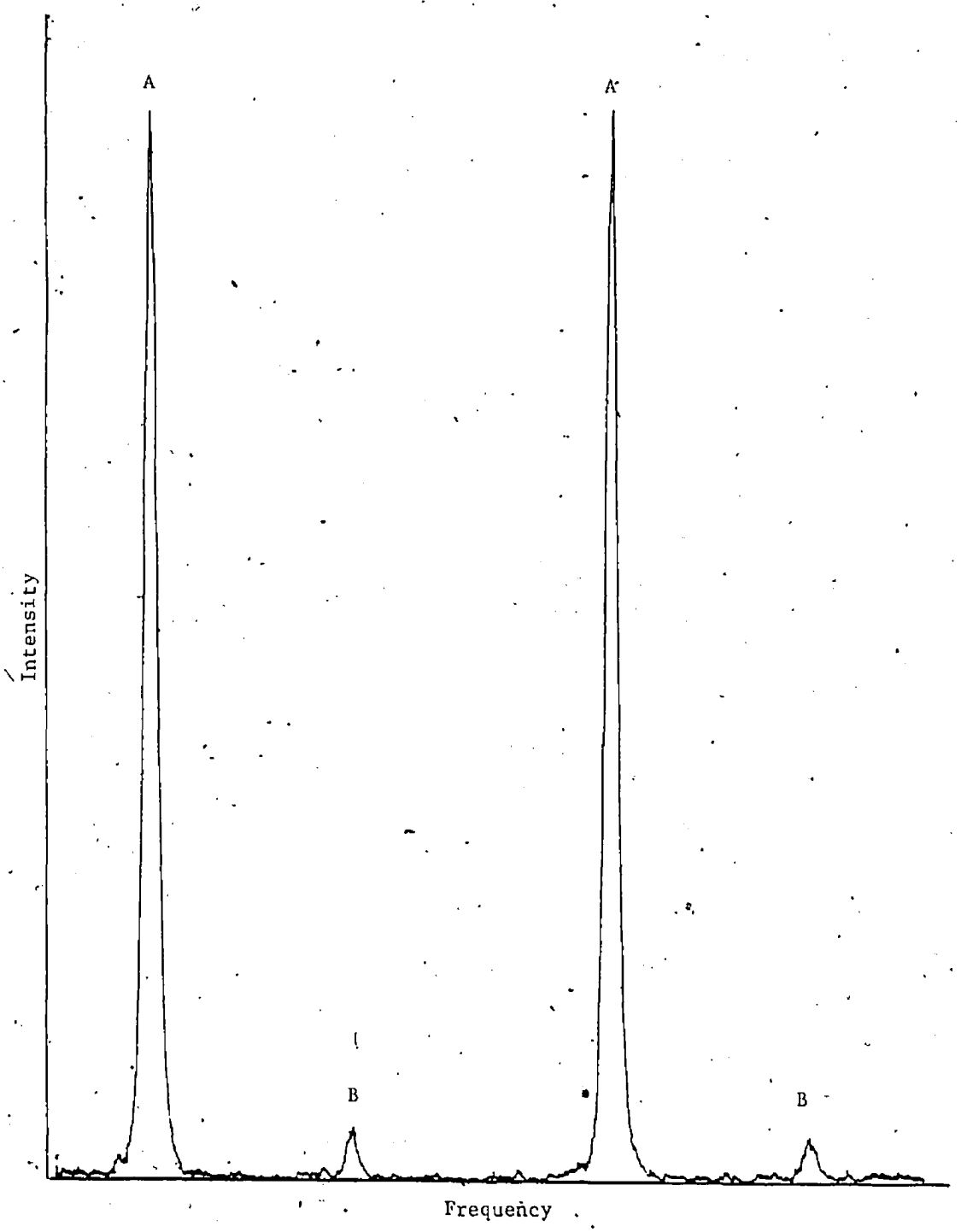

Five experimental runs were carried out, two with H_2, two with N_2 and one with Ar, each run covering the approximate pressure range 0.1 - 0.9 torr. The interferograms of the fluorescent Zeeman spectra, corresponding to the transitions shown in Fig. 3, covered three interference orders. The peaks corresponding to the components that belong to the two fine-structure states occur in different orders, however the mirror separation was adjusted to make the two orders overlap. This allowed each interferometer scan to cover three full interference orders for each fine-structure state.

Figure 5 shows an actual trace of two of the interference orders obtained with Ar, which is characterized by the relatively intense A and B components (corresponding to the A and B transitions in Fig. 3). Component B, even after subtracting σ^+ leakage, is still more intense than components C, D, E and F which arise from the collisionally populated $^2P_{3/2}$ state. This is due to the fact that the cross sections for fine-structure mixing by collisions with Ar are relatively small (Ciurylo and Krause, 1983). Figure 6 shows a spectral trace for the K-N_2 system. It differs from that obtained with Ar by the relatively stronger C, D, E and F components which are due to the larger fine-structure mixing cross sections. The intensities of the A and B components in Figs. 5 and 6 are quite similar. Since the masses and relative collision speeds in the two cases are also comparable, it follows that the two cross sections for $^2P_{\frac{1}{2}\,-\frac{1}{2}} \rightarrow {}^2P_{\frac{1}{2}\frac{1}{2}}$ Zeeman mixing and hence the multipole relaxation cross sections are of similar magnitude. Figure 7 shows the spectrum obtained with H_2 as buffer gas. Although the relative intensities of the Zeeman components appear comparable to those in Fig. 6, it should be noted

Fig. 5 A trace of the Zeeman fluorescent spectrum emitted from K vapour mixed with 0.548 torr Ar. The $4^2P_{\frac{1}{2}} - {}^{\frac{1}{2}}$ state is optically excited. The peaks are labelled to correspond to the transitions indicated in Fig. 3.

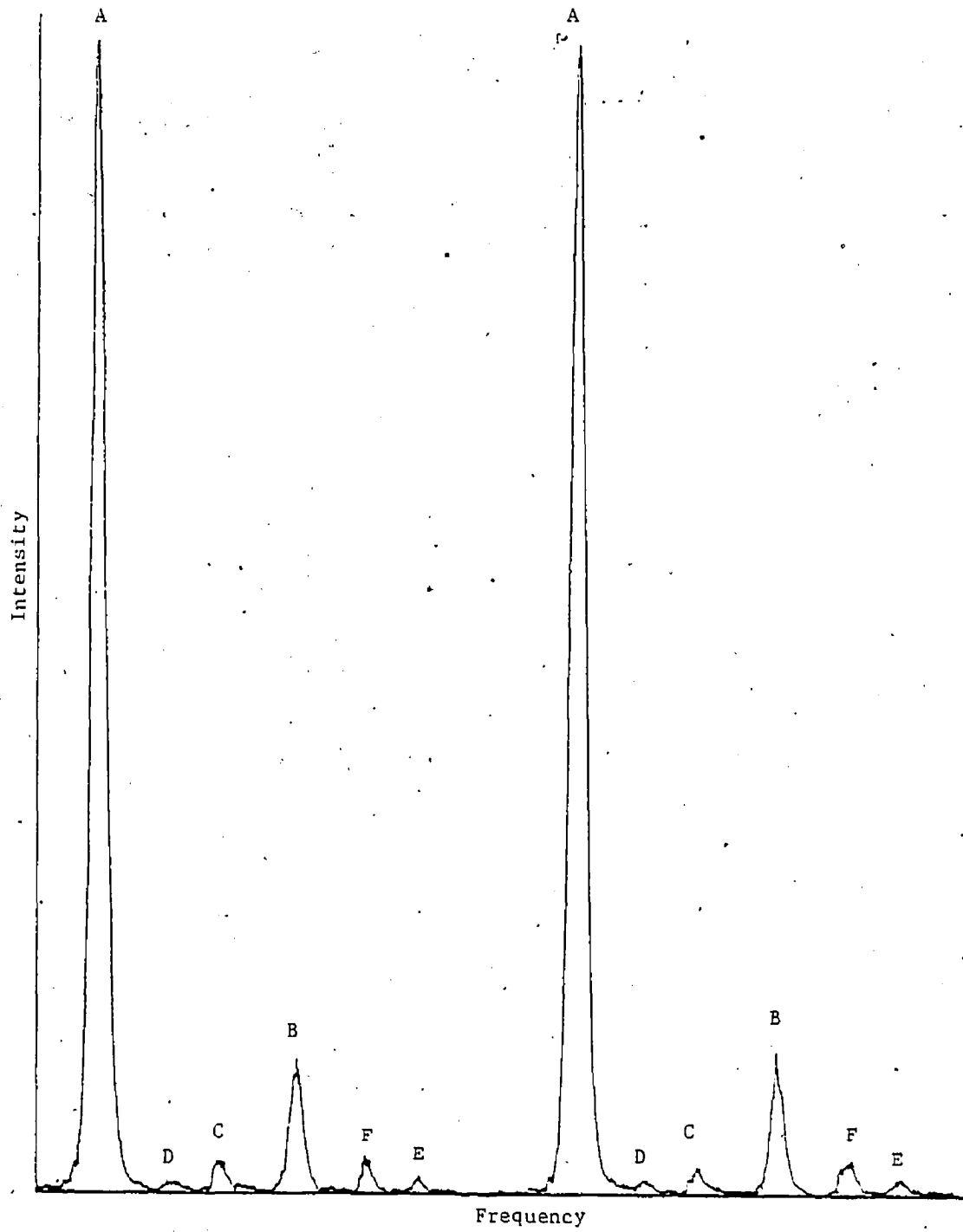

Fig. 6 A trace of the Zeeman fluorescent spectrum emitted from K vapour mixed with 0.411 torr N_2. The $4^2P_{\frac{1}{2}\ -\frac{1}{2}}$ state is optically excited. The peaks are labelled to correspond to the transitions indicated in Fig. 3.

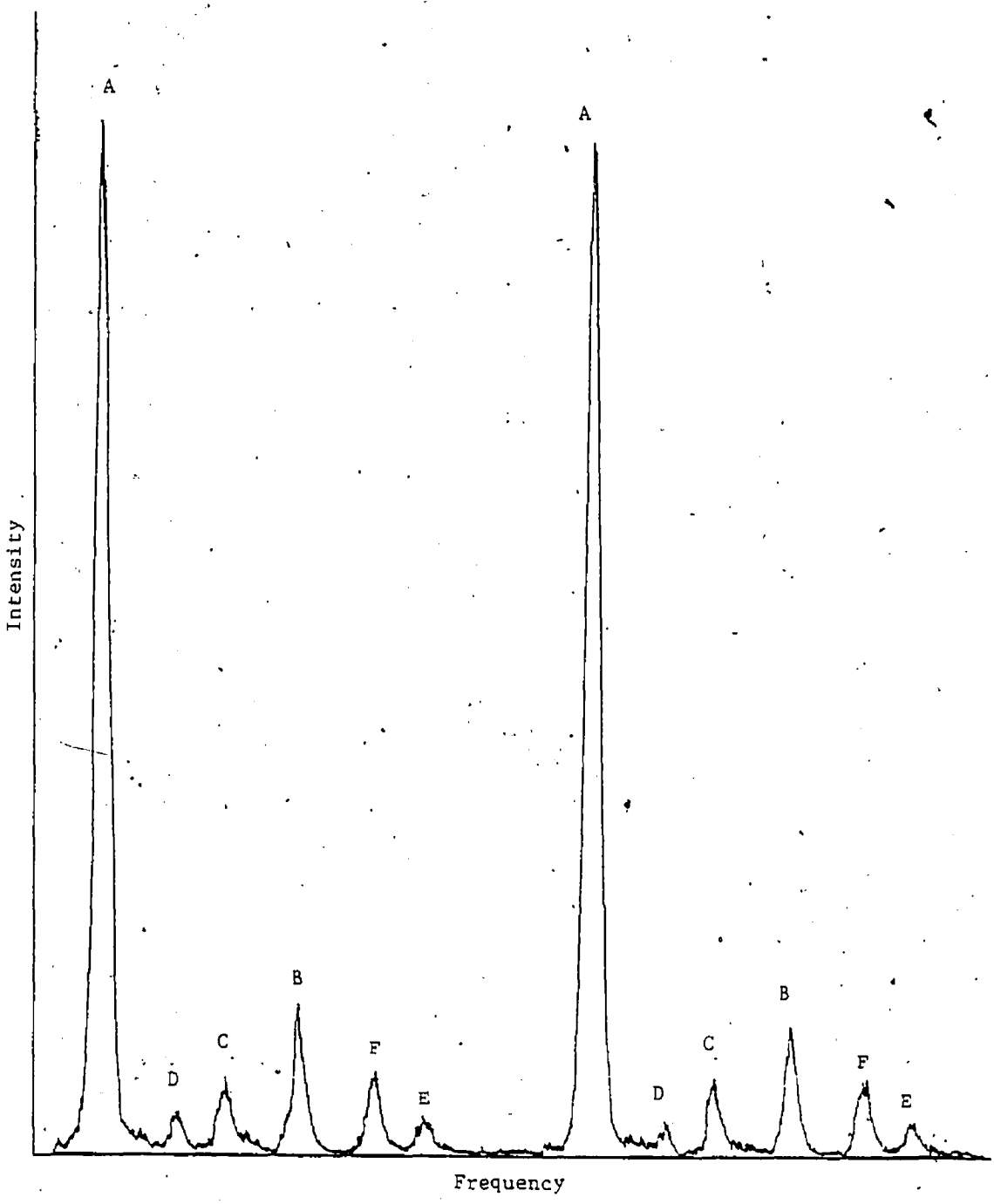

Fig. 7 A trace of the Zeeman fluorescent spectrum emitted from K vapour mixed with 0.115 torr H_2. The $4^2P_{\frac{1}{2}}$ $-\frac{1}{2}$ state is optically excited. The peaks are labelled to correspond to the transitions indicated in Fig. 3.

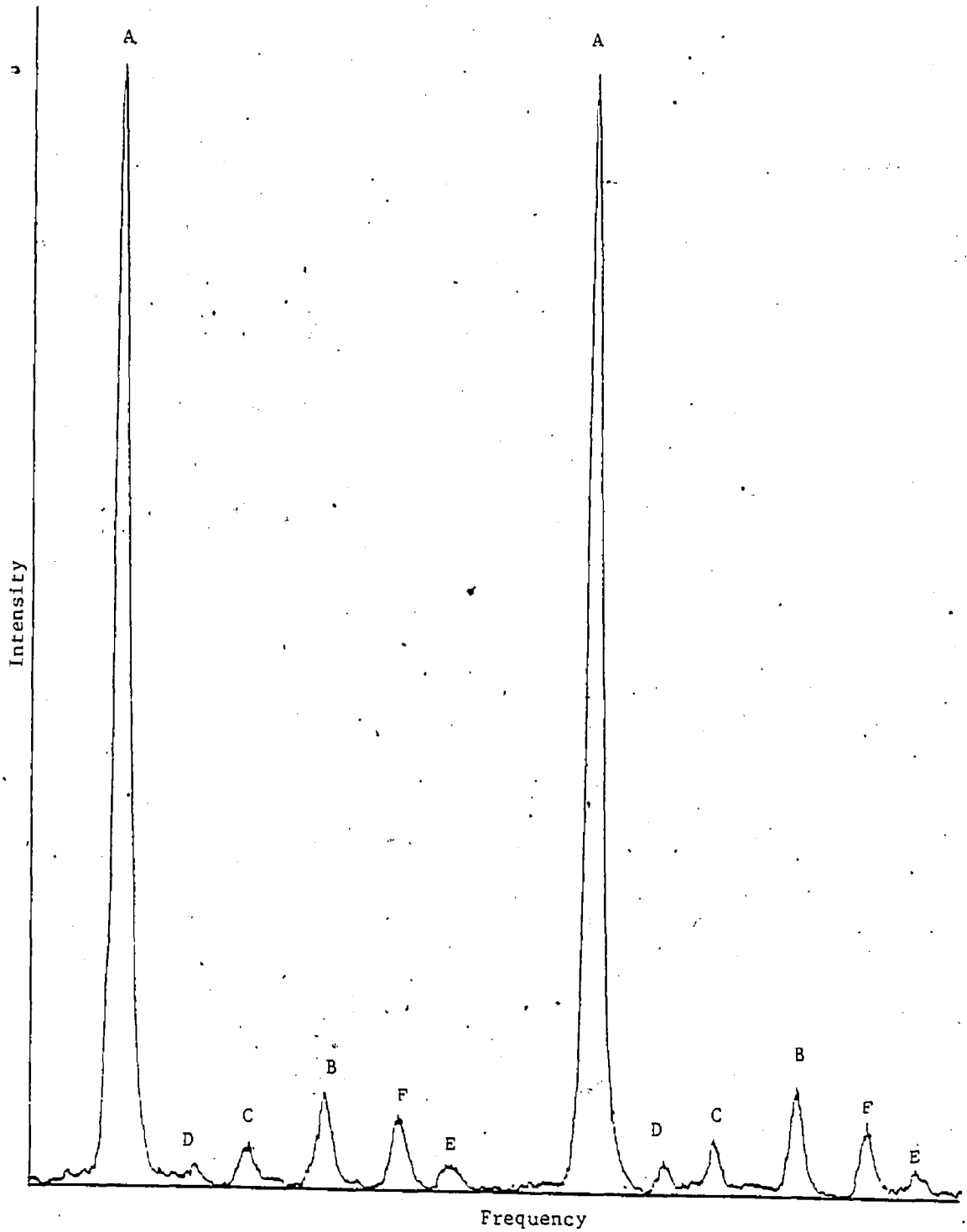

that the H_2 pressure was considerably lower than the N_2 pressure in Fig. 6. The larger relative speed of the K-H_2 collision partners is reflected by the relatively strong Zeeman intensities obtained at relatively low H_2 pressure.

Figure 8 shows the various radiative Zeeman transitions resulting from the selective excitation of the $4^2P_{3/2\ -3/2}$ Zeeman substate in potassium in the presence of a buffer gas. Here the components D', E' and F' arise primarily from the collisional Zeeman mixing within the $^2P_{3/2}$ fine-structure state and A' and B' are due to fine-structure mixing. Again, a small amount of σ^+ leakage was observed which caused the $^2P_{3/2\ 3/2}$ state to be populated directly, and consequently the peak F' in each of these spectra included the intensity arising from collisional excitation transfer as well as that from direct optical excitation resulting from this σ^+ leakage (depicted in Fig. 9).

Figure 10 represents a trace of the fluorescent Zeeman spectrum obtained with Ar, with the various peaks labelled to correspond to the transitions in Fig. 8. The relative intensities of the peaks C', D', E' and F' are considerably higher than those of the peaks A' and B', because of the small fine-structure mixing cross section. Figures 11 and 12 show the corresponding spectra obtained with N_2 and H_2. Because the fine-structure mixing cross sections for these gases is relatively large, the peaks B' and E' are of comparable height, while for Ar peak E' is noticeably higher than B'. Where two components in the spectrum overlapped, as for example the peaks B' and E' in Fig. 10, their relative intensities were obtained from the traces by making appropriate corrections for the overlap.

Fig. 8 Energy level diagram of the K^2P Zeeman substates showing their σ decays to the ground state. The $4^2P_{3/2}$ $-3/2$ substate is optically populated, the other substates are populated by collisions. The π transitions are not shown; the spacings between energy levels are not drawn to scale.

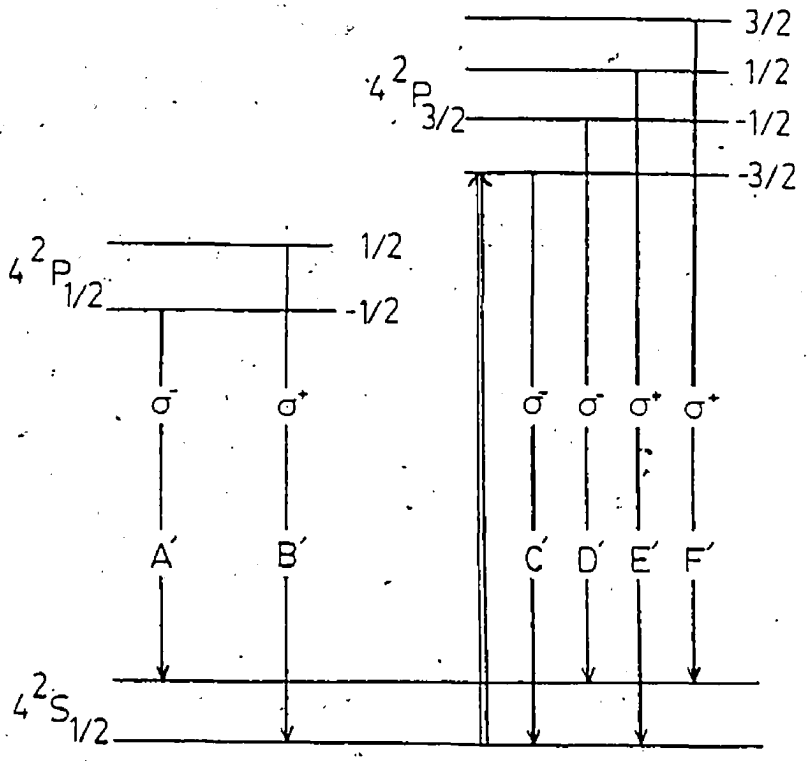

Fig. 9 A trace of the fluorescent spectrum emitted from pure K vapour, undergoing $4^2P_{3/2}$ $-3/2$ excitation. Peak F', as labelled in Fig. 8, arises from σ^+ leakage through the polarizers.

Fig. 10 A trace of the Zeeman fluorescent spectrum emitted from K vapour mixed with 0.884 torr Ar. The $4^2P_{3/2\ -3/2}$ substate is optically excited. The peaks are labelled to correspond to the transitions indicated in Fig. 8.

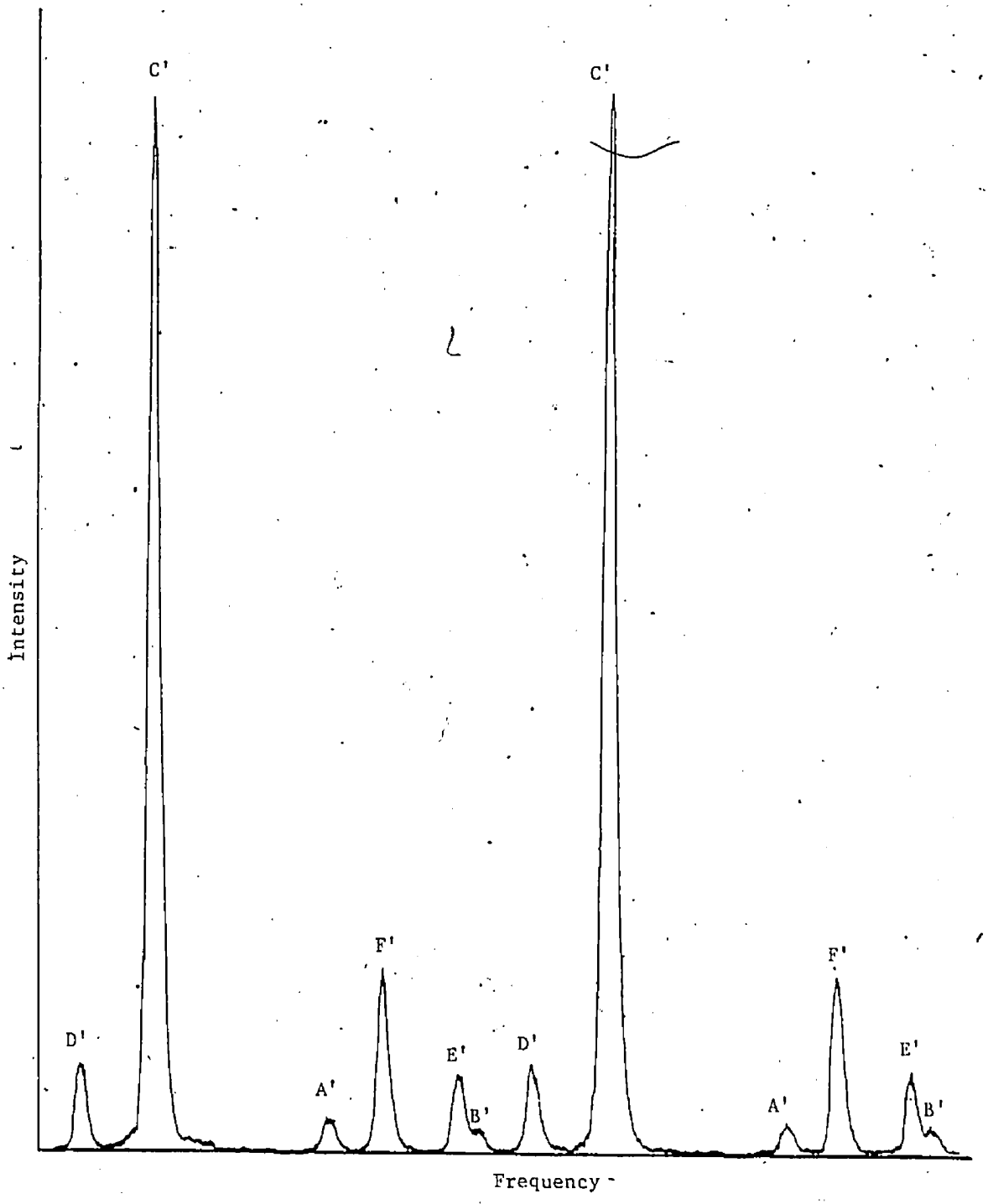

Fig. 11 A trace of the Zeeman fluorescent spectrum emitted from K vapour mixed with 0.310 torr N_2. The $4^2P_{3/2}$-3/2 substate is optically excited. The peaks are labelled to correspond to the transitions indicated in Fig. 8. A 3x magnified trace of the collisionally induced components is also shown.

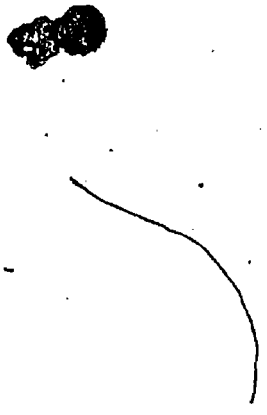

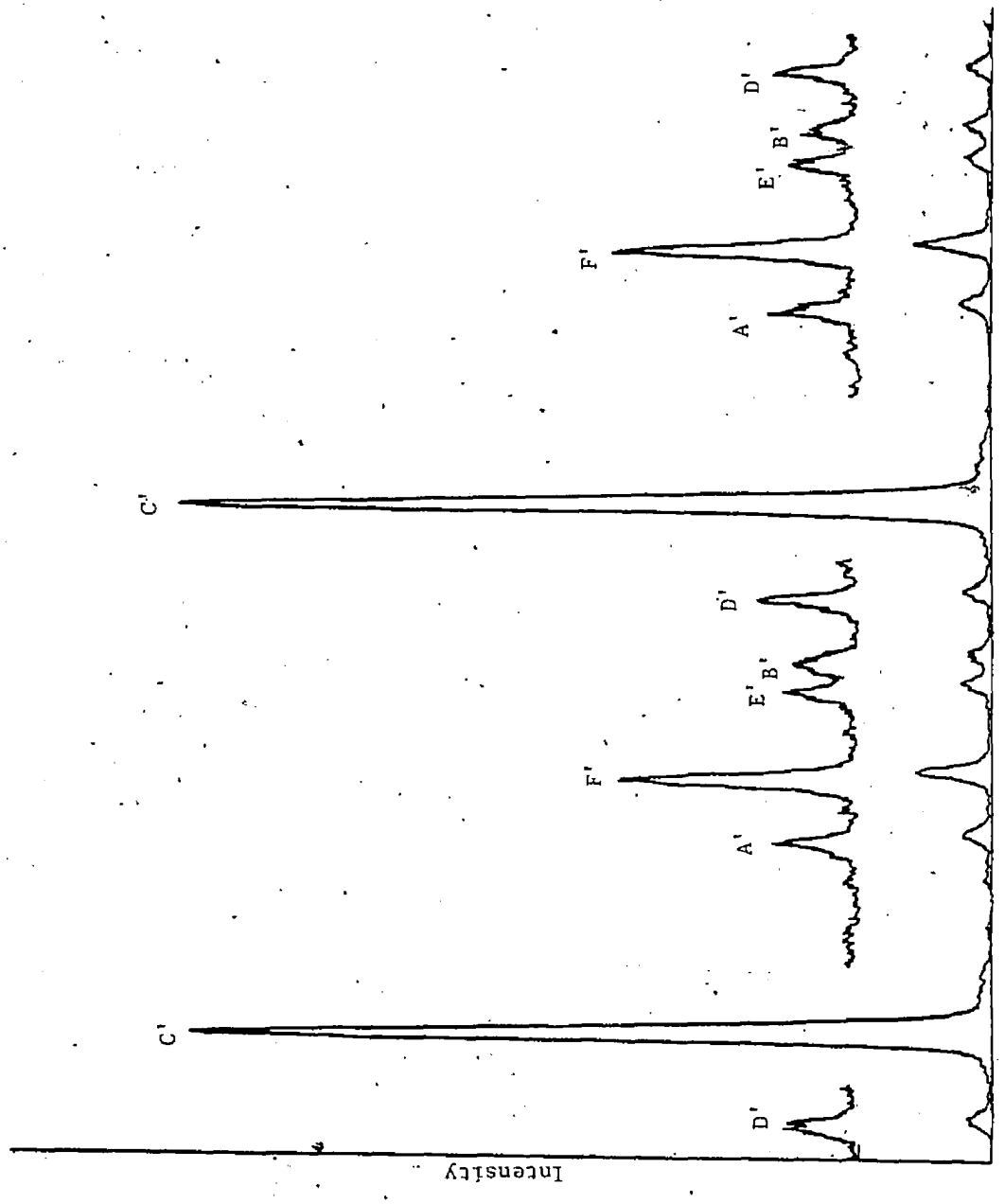

Fig. 12 A trace of the Zeeman fluorescent spectrum emitted from K vapour mixed with 0.353 torr H_2. The $4^2P_{3/2}$ -3/2 substate is optically excited. The peaks are labelled to correspond to the transitions indicated in Fig. 8.

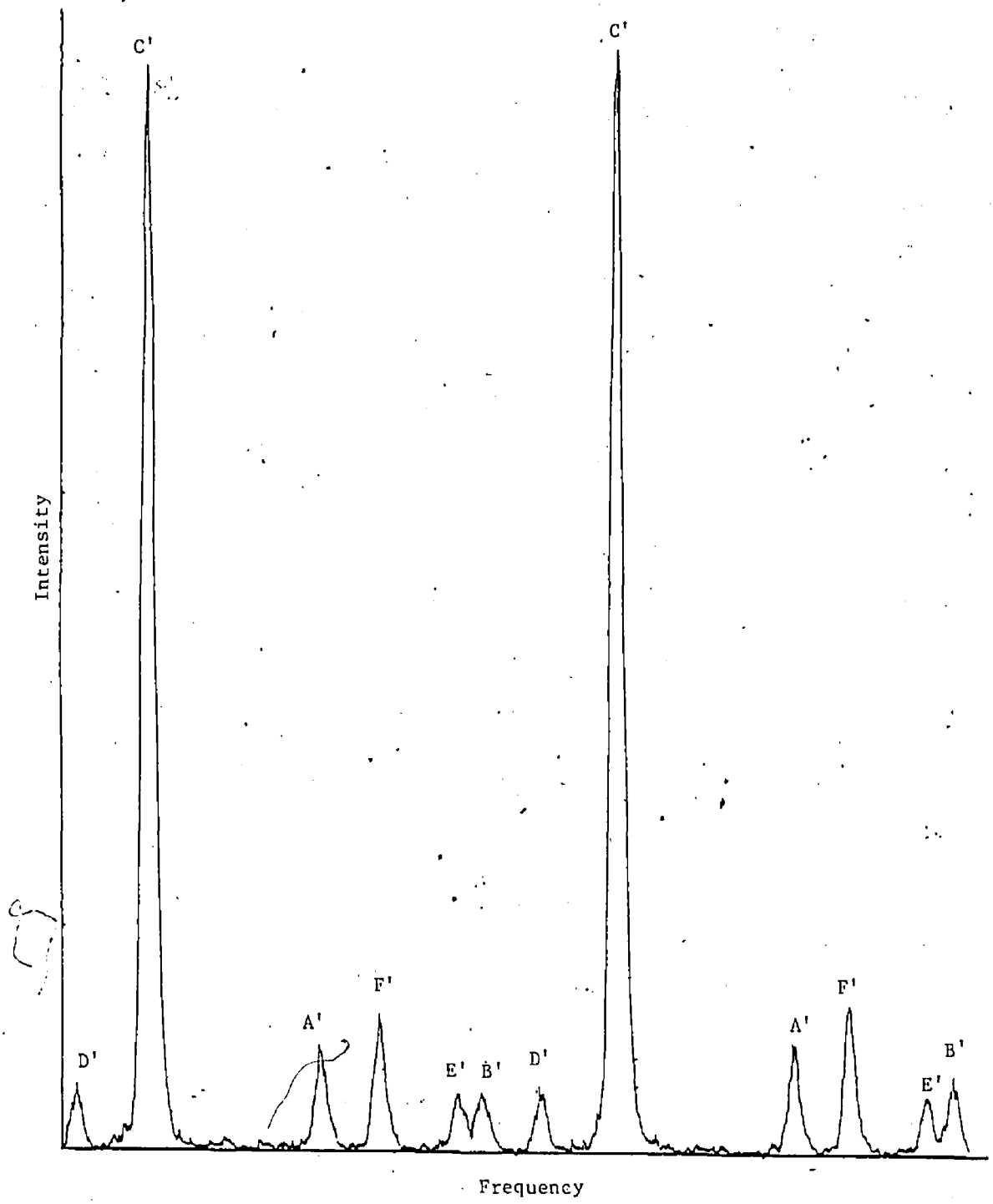

2. Determination of Multipole Relaxation Cross Sections From the Zeeman Spectra

The peak intensities of all the components in the traces of the Zeeman fluorescent spectra, scanned through three interference orders, were individually measured and the ratios of the intensities of the components arising from the collisionally populated states relative to those of the optically excited states were calculated.

The percentage of σ^+ leakage (approximately 3.6%) was determined from the average of numerous scans of pure K vapour, such as those shown in Figs. 4 and 9, taken during each experimental run and the affected intensity ratios $\frac{I(B)}{I(A)}$ and $\frac{I(F')}{I(C')}$ were corrected appropriately.

The measured intensity ratios were multiplied by the appropriate numerical factors according to eq. (66) to relate them to the ratios of the actual populations of the Zeeman states. These ratios were plotted in relation to $N\bar{v}\tau$, where $\tau = \tau_1$ for intensity ratios $\frac{I(B)}{I(A)}$, $\frac{I(A')}{I(C')}$ and $\frac{I(B')}{I(C')}$ and $\tau = \tau_2$ for all other ratios, in order to account for the variation in the collision speed among the buffer gases as well as for the effects of radiation trapping (Skalinski, 1982).

Figures 13 and 14 are the plots of the population (and intensity) ratios obtained with Ar as a buffer gas. The plots are quite linear at low pressures and some exhibit a slight downward curvature as the pressure increases. At low densities the time between successive collisions exceeds the lifetime of the ^2P states and the intensity ratio plots are expected to be linear since at most a single collisional process may be observed during the lifetime of the 4^2P state. At higher pressures above about 0.3 torr (7×10^{15} cm^{-3}) the curvature indicates the presence of effects due to multiple collisional transfers, which are most

Fig. 13 Plots of Zeeman fluorescent intensity ratios arising from $4^2P_{\frac{1}{2}} - \frac{1}{2}$ excitation, showing effects of Zeeman mixing induced in K-Ar collisions. The separate origin for each plot is indicated on the vertical axis. The pressure scale shown is approximate. The error bars represent statistical scatter of the measurements.

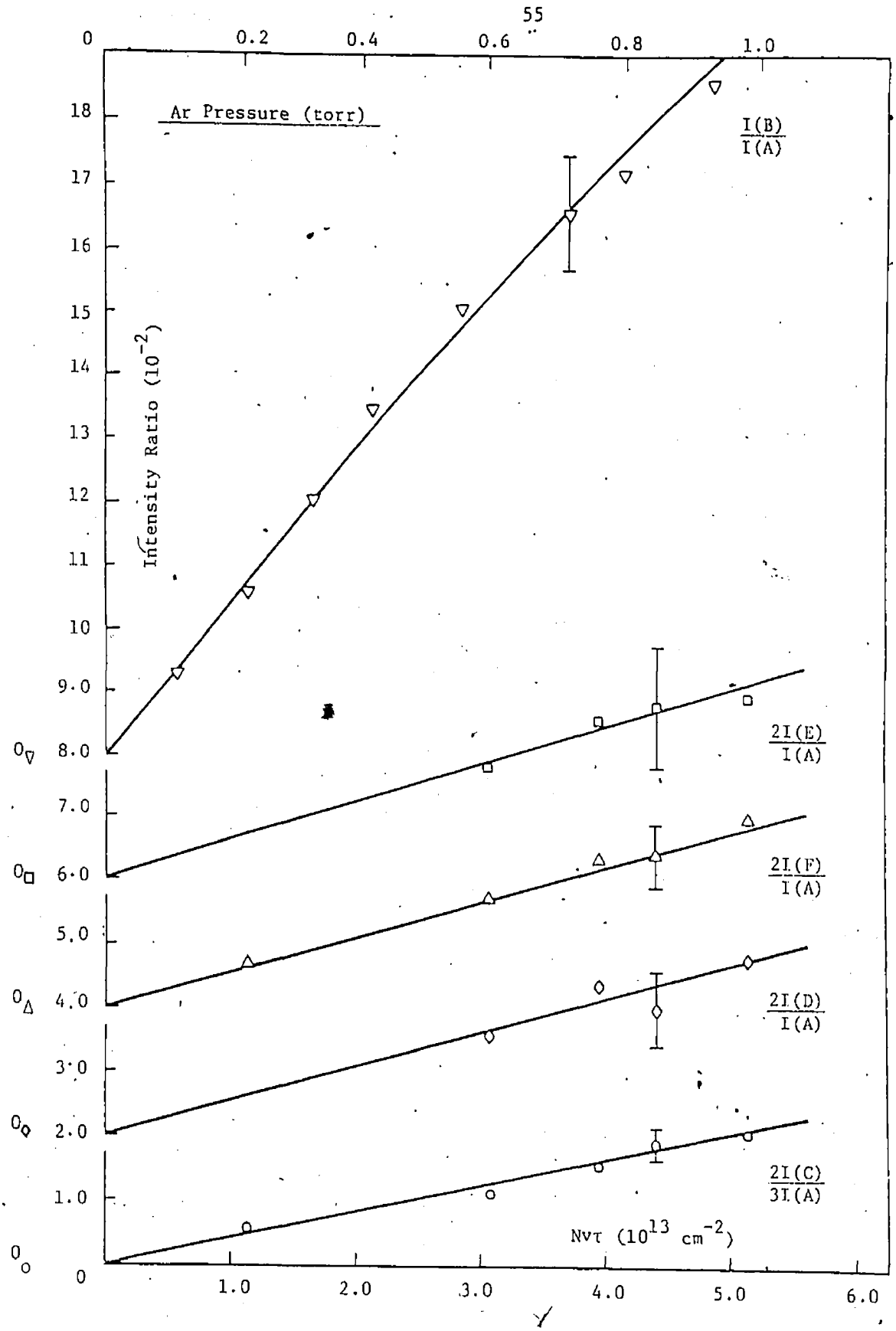

Fig. 14 Plots of Zeeman fluorescent intensity ratios arising from $4^2P_{3/2\ -3/2}$ excitation, showing effects of Zeeman mixing induced in K-Ar collisions. The separate origin for each plot is indicated on the vertical axis. The pressure scale shown is approximate. The error bars represent statistical scatter of the measurements.

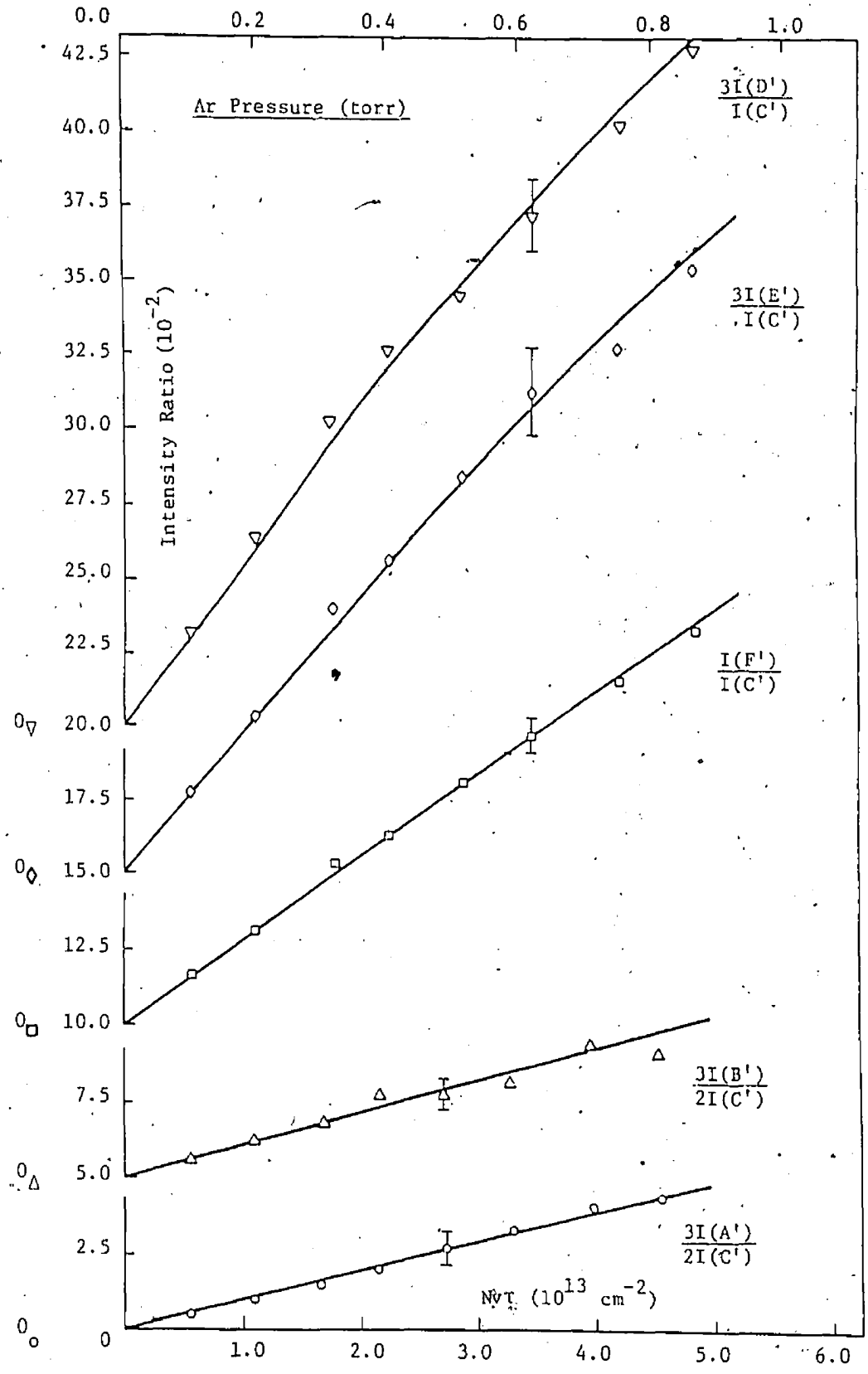

noticeable within the directly populated fine-structure state, where the separation between the Zeeman substates is small compared to the larger fine-structure splitting (57 cm^{-1}) between the potassium $^2P_{1/2}$ and $^2P_{3/2}$ states. These characteristics also apply to the plots for N_2 (shown in Figs. 15 and 16) and the plots for H_2 (Figs. 17 and 18). The plots for H_2 exhibit a noticeably larger degree of curvature than those for Ar because the relative collision speed is larger. The linearity of the plots for argon indicates that single-collision conditions are applicable to this system over almost the whole pressure range, while in the case of H_2 only the data obtained in the linear region of the plots are taken under single-collision conditions.

In order to determine a value for the orientation transfer cross section $\sigma_{12}^{(1)}$ and $\sigma_{21}^{(1)}$ for N_2 and H_2 the appropriate intensity ratios in the linear region of the plots were substituted into eq. (77) to determine the Zeeman transfer cross sections $Q(Jm \rightarrow J'm')$. The difference of the appropriate Q values (eqs. (79)-(81)) yields $\sigma_{12}^{(1)}$ and $\sigma_{21}^{(1)}$. The large uncertainty in these cross sections as well as their relatively small sizes, which may be seen in Table 1, justify the simplification of the theoretical treatment discussed in Chapter I by neglecting the product $\sigma_{12}^{(1)}\ \sigma_{21}^{(1)}$ and thus the product $\gamma_{12}^{(1)}\ \gamma_{21}^{(1)}$ in eqs. (73) and (74).

The appropriate intensity ratios together with their corresponding values of $N\bar{v}\tau$ were substituted into eqs. (68)-(72) to obtain the $K_{ab}^{LL'}$ values corresponding to each $N\bar{v}\tau$ value. These were then substituted in eqs. (82) and (83) along with $\sigma_{11}^{(0)}$ and $\sigma_{22}^{(0)}$ obtained by eqs. (45) and (46) from the $\sigma_{12}^{(0)}$ and $\sigma_{21}^{(0)}$ values of Ciurylo and Krause (1982, 1983), as listed in Table 2, in order to obtain the multipole relaxation cross

Fig. 15 Plots of Zeeman fluorescent intensity ratios arising from $4^2P_{\frac{1}{2}} - \frac{1}{2}$ excitation, showing effects of Zeeman mixing induced in K-N_2 collisions. The separate origin for each plot is indicated on the vertical axis. The pressure scale shown is approximate. The error bars represent statistical scatter of the measurements.

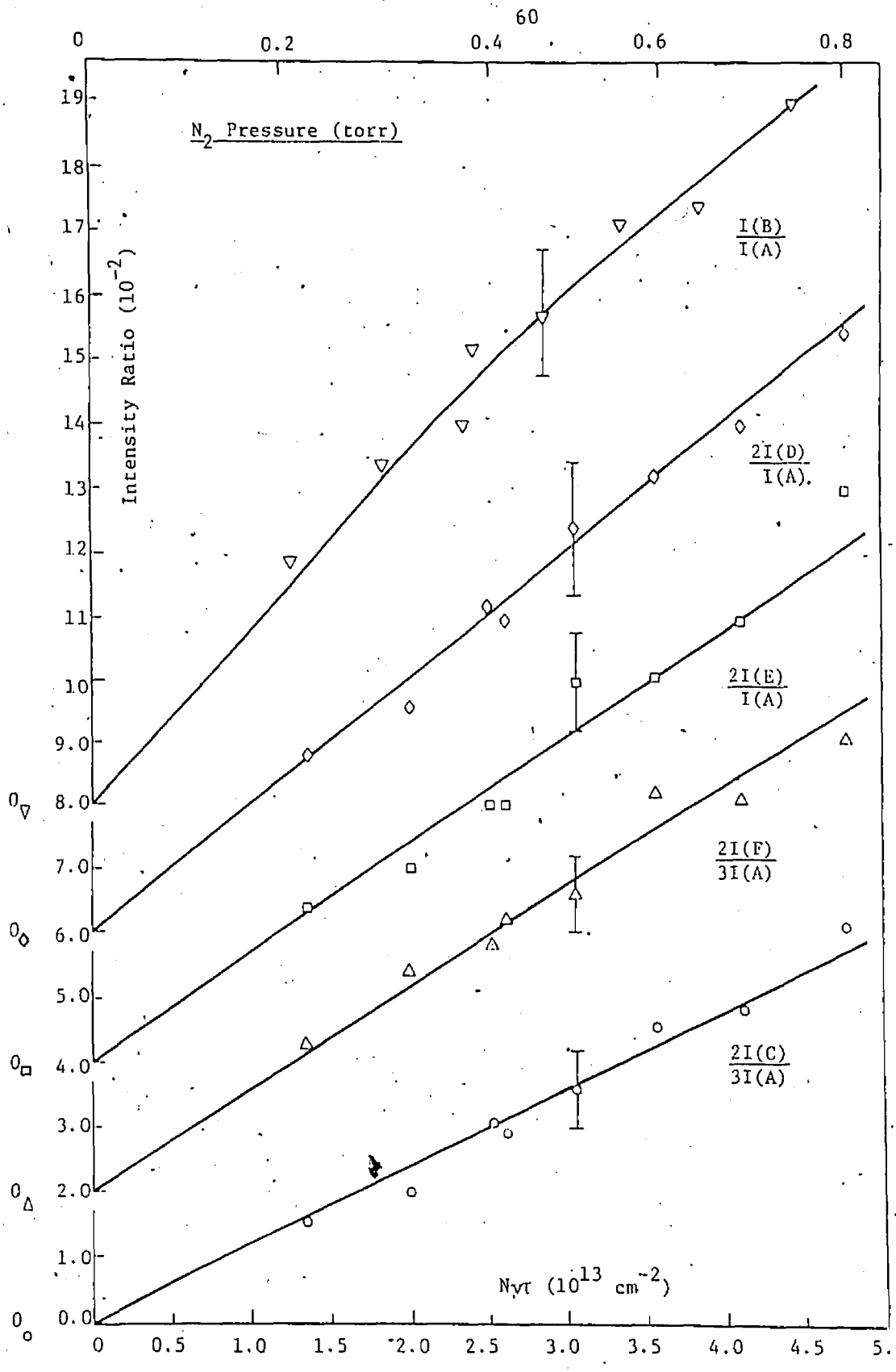

Fig. 16 Plots of Zeeman fluorescent intensity ratios arising from $4^2P_{3/2\ -3/2}$ excitation, showing effects of Zeeman mixing induced in K-N_2 collisions. The separate origin for each plot is indicated on the vertical axis. The pressure scale shown is approximate. The error bars represent statistical scatter of the measurements.

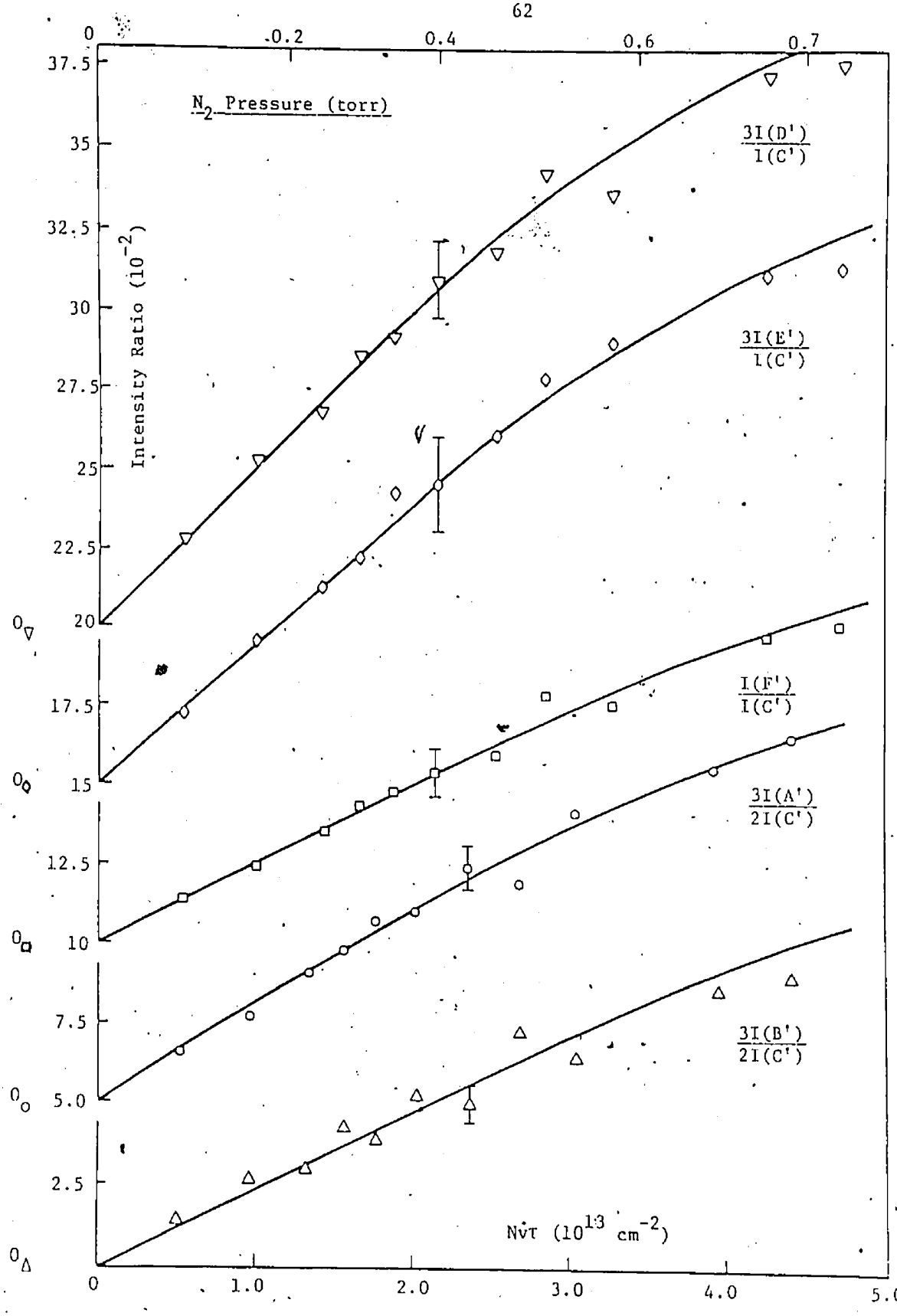

Fig. 17 Plots of Zeeman fluorescent intensity ratios arising from $4^2P_{\frac{1}{2}} - \frac{1}{2}$ excitation, showing effects of Zeeman mixing induced in K-H_2 collisions. The separate origin for each plot is indicated on the vertical axis. The pressure scale shown is approximate. The error bars represent scatter of the measurements.

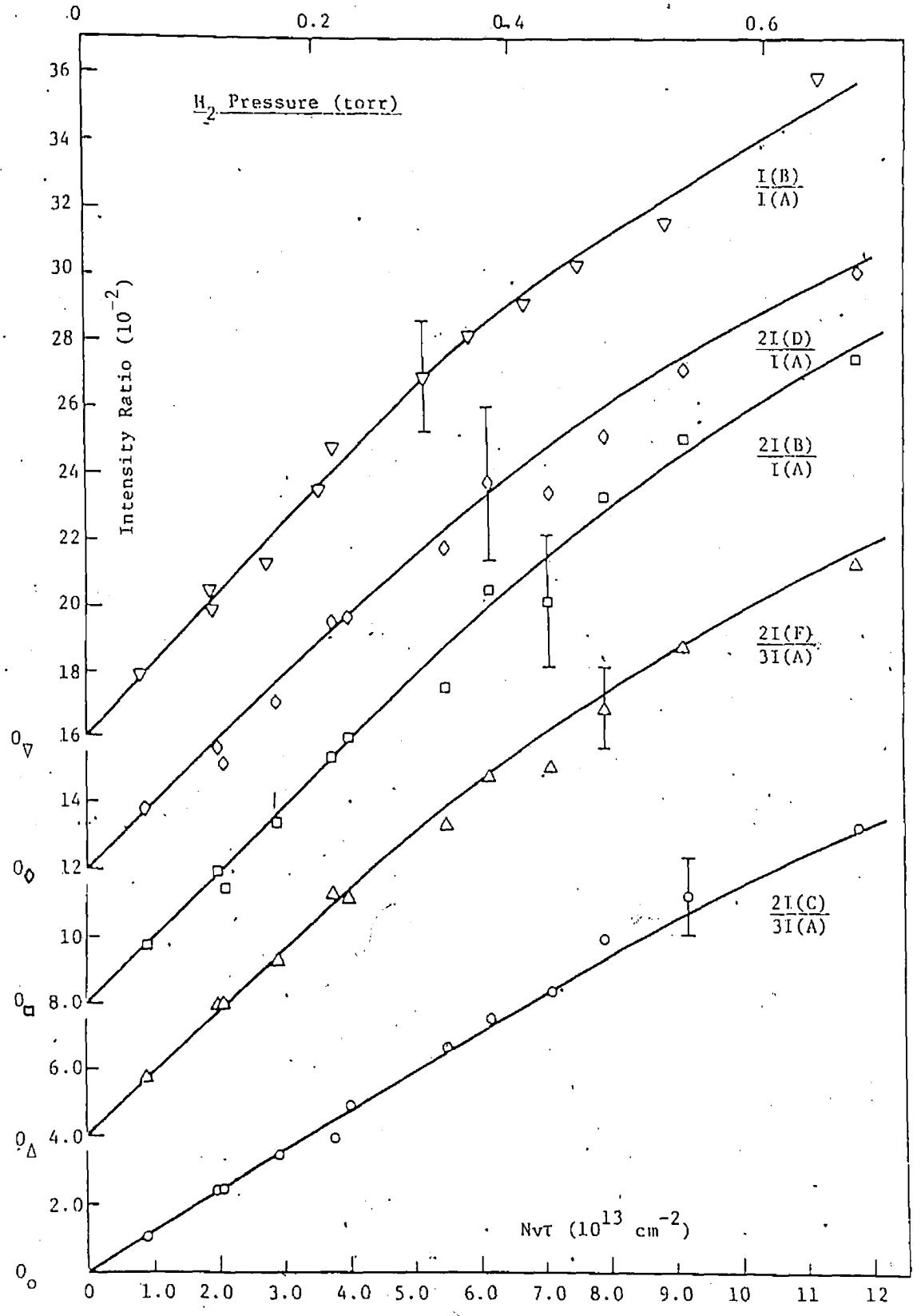

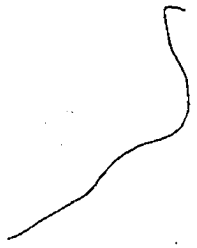

Fig. 18 Plots of Zeeman fluorescent intensity ratios arising from $4^2P_{3/2\ -3/2}$ excitation, showing effects of Zeeman mixing induced in K-H_2 collisions. The separate origin for each plot is indicated on the vertical axis. The pressure scale shown is approximate. The error bars represent statistical scatter of the measurements.

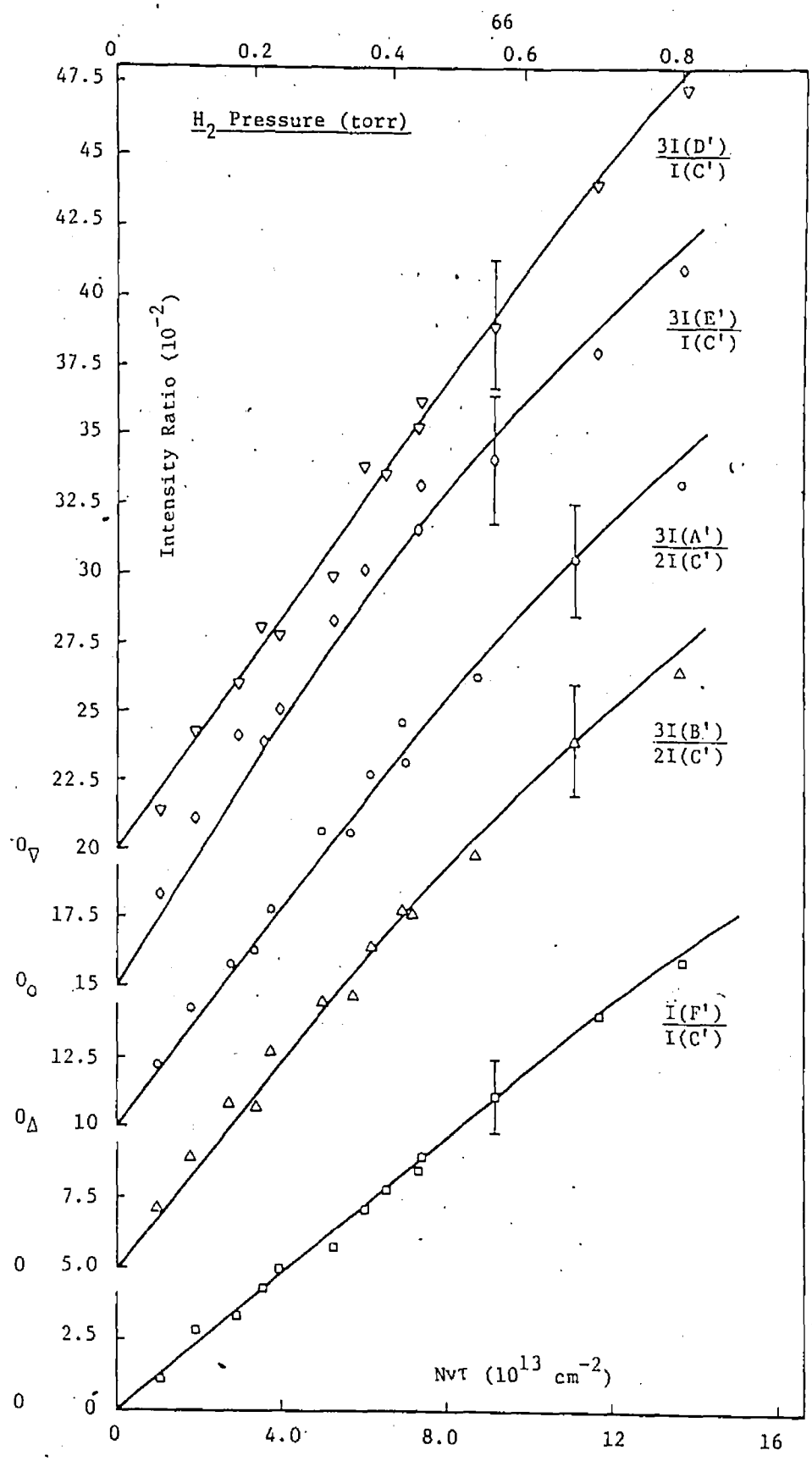

TABLE 1

CROSS SECTIONS FOR ORIENTATION TRANSFER BETWEEN $4^2P_{1/2}$ AND $4^2P_{3/2}$ STATES

Buffer Gas	$\sigma_{12}^{(1)}(10^{-16}\ cm^2)$	$\sigma_{21}^{(1)}(10^{-16}\ cm^2)$
N_2	6.1 ±3.4	1.3 ±6
H_2	1.6 ±1	3.4 ±4

TABLE 2

CROSS SECTIONS FOR $4^2P_{1/2} \leftrightarrow 4^2P_{3/2}$ MIXING, INDUCED IN COLLISIONS WITH Ar, N_2 AND H_2

Buffer Gas	$\sigma_{12}^{(0)}(1/2 \rightarrow 3/2)$ $(10^{-16}cm^2)$	$\sigma_{21}^{(0)}(1/2 \leftarrow 3/2)$ $(10^{-16}cm^2)$	$\sigma_{11}^{(0)}$ c $(10^{-16}cm^2)$	$\sigma_{22}^{(0)}$ c $(10^{-16}cm^2)$
Ar	16 ±2.4 [a]	11.2 ±1.7 [a]	11.3 ±1.7	15.8 ±2.4
N_2	79 ±12 [b]	54 ±8 [b]	55.9 ±8.5	76.4 ±11.3
H_2	57 ±9 [b]	39 ±6 [b]	40.3 ±6.4	55.1 ±8.5

a Ciurylo and Krause, 1982

b Ciurylo and Krause, 1983

c $\sigma_{11}^{(0)}$ and $\sigma_{22}^{(0)}$ were determined from $\sigma_{12}^{(0)}$ and $\sigma_{21}^{(0)}$ using eqs. (45) and (46)

sections $\Lambda_{1/2}^{(1)}$ and $\Lambda_{3/2}^{(L)}$. The latter were averaged over all NVT values, and the resulting averages are listed in Table 3 together with the $\Lambda_J^{(L)}$ measured for argon by Skalinski and Krause (1982).

The multipole relaxation cross sections for argon were calculated from the data taken during one experimental run as a test of the experimental system. The agreement between the values determined by Skalinski and Krause (1982) and the values determined in this experiment is quite adequate and within experimental error. The largest relative discrepancy occurs with $\Lambda_{1/2}^{(1)}$, which is probably due to the fairly large uncertainty in the correction for σ^+ leakage. One general difference between the two experiments is that of the effects of fine-structure mixing. Noble gas atoms induce considerably less fine-structure mixing than the molecules N_2 and H_2 (Ciurylo and Krause, 1982, 1983) and to a good approximation the fine-structure mixing may be neglected in K-noble gas collision systems. $\Lambda_{1/2}^{(1)}$ for N_2 is of similar magnitude as this value for Ar. The value of $\Lambda_{1/2}^{(1)}$ reported by Sieradzan and Franz (1982) for Rb-N_2 collisions is larger than that for the K-N_2 collision system. The values of $\Lambda_{3/2}^{(L)}$ for K-N_2 and K-Argon interactions are very similar in magnitude while for H_2 these values are approximately 50% smaller, this difference may be attributable to the relative sizes of the collision partners. The total multipole decay cross sections, as defined by eqs. (53) and (54), reflects both relaxation and fine-structure mixing, and are listed in Table 4.

3. Sources of Experimental Error

The total contribution of the systematic and statistical uncertainties present in the experiment to the final values of the multipole relaxation

TABLE 3

MULTIPOLE RELAXATION CROSS SECTIONS FOR COLLISIONS WITH Ar, N_2 and H_2

Buffer Gas	$\Lambda^{(1)}_{\frac{1}{2}}(10^{-16}cm^2)$	$\Lambda^{(1)}_{3/2}(10^{-16}cm^2)$	$\Lambda^{(2)}_{3/2}(10^{-16}cm^2)$	$\Lambda^{(3)}_{3/2}(10^{-16}cm^2)$
Ar [a]	52 ±9	169.4 ±25	250 ±38	203 ±30
Ar [b]	65 ±10	175 ±25	230 ±35	190 ±30
N_2 [a]	58.7 ±9	154.6 ±23	228.3 ±34	173.6 ±26
H_2 [a]	46 ±7	80 ±12	125 ±19	66 ±15
Rb–N_2 [c]	105 ±25			

a This investigation

b Skalinski and Krause, 1982

c Sieradzan and Franz, 1982

TABLE 4

MULTIPOLE DECAY CROSS SECTIONS FOR COLLISIONS WITH Ar, N_2 AND H_2

Buffer Gas	$\sigma_{11}^{(1)}(10^{-16}cm^2)$	$\sigma_{22}^{(1)}(10^{-16}cm^2)$	$\sigma_{22}^{(2)}(10^{-16}cm^2)$	$\sigma_{22}^{(3)}(10^{-16}cm^2)$
Ar	64 ±9	185 ±25	266 ±38	219 ±30
N_2	115 ±19	231 ±26	305 ±36	250 ±28
H_2	86 ±9	135 ±15	181 ±21	121 ±17

cross sections has been estimated to be within the limits of ±15%. The systematic errors affecting the values of the multipole relaxation cross sections are primarily associated with the temperature and pressure measurements. The temperatures of the side arm and main oven were measured by a thermocouple system which was referenced to $0^{\circ}C$ using an insulated container of ice. The reference zero of this system was affected by the various contact potentials generated in the system by oxidation layer formation on the contacts and by the sensitivity of the thermocouple network to the r.f. energy emitted from the r.f. oscillator operating the lamp. These effects were minimized but could not be entirely eliminated. The presence of a thermal gradient in the potassium contained in the side arm of the cell as well as the small variations in the temperature of the side arm due to the ultrathermostat affect the determination of the vapour pressure from the temperature-vapour pressure relation (Nesmeyanov, 1963). The approximate nature of the vapour pressure relation based on experimental data, also contributes to a systematic uncertainty in the potassium vapour pressure which affects the radiation trapping correction. It has been assumed that the vapour pressure in the cell is the same as in the side arm, irrespective of the fact that the oven is at a higher temperature than the side arm. The buffer gas pressure uncertainty stems from the fact that the pressure was measured at room temperature while the cell into which the gas was admitted was at a higher temperature ($\sim 110^{\circ}C$). It was assumed that there was no difference between the measured pressure and the actual pressure since the gas pressures were believed to be sufficiently high to avoid transpiration effects. The main source of statistical error is due to the fluctuations

in the lamp intensity. Although the monitored intensity of the lamp remained quite stable over long periods of time, any small fluctuations in the signal contribute significantly to the measured spectral intensity ratios, as the ratio of a small signal to a larger signal is affected more by the variation in the small signal than the variation in the much larger signal. At each gas pressure the spectrum was scanned several times and the resulting average intensity ratios had a statistical variation of about ±10%, which is represented by the statistical error bars in Figs. 13-18.

The correction for σ^+ leakage was determined by averaging the values obtained from the spectral recordings taken with the cell evacuated such as those shown in Figs. 4 and 9. The statistical fluctuation in these ratios also contribute to the statistical error present in the corrected values of the $\frac{I(\frac{1}{2}\frac{1}{2})}{I(\frac{1}{2}\ -\frac{1}{2})}$ and $\frac{I(3/2\ 3/2)}{I(3/2\ -3/2)}$ ratios, as the σ^+ leak at low buffer gas pressures was comparable in size to these corrected ratios. Any effects due to quenching of radiation has also been neglected in this experiment. The consideration of these various uncertainties yield an approximate bound on the uncertainty in the final values of the multipole relaxation cross sections of ±15%.

BIBLIOGRAPHY

Baylis, W. E. 1979 in Progress in Atomic Spectroscopy, Part B, W. Hanle and H. Kleinpoppen, Eds., Plenum Publishing Corp., New York

Baylis, W. E. 1983 Private Communication

Berdowski, W. and Krause, L. 1968 Phys. Rev. 165, 158.

Berdowski, W., Shiner, T. and Krause, L. 1971 Phys. Rev. A 4, 984.

Burgmans, A. L. 1979 Phys. Rev. A 19, 1954.

Boggy, R. and Franz, F. A. 1982 Phys. Rev. A 25, 1887.

Bulos, R. B. and Happer, W. 1971 Phys. Rev. A 4, 849.

Ciurylo, J. and Krause, L. 1982 J.Q.S.R.T. 28, 457.

Ciurylo, J. and Krause, L. 1983 J.Q.S.R.T. 29, 57.

Copley, G. and Krause, L. 1969 Can. J. Phys. 47, 533.

Dyakonov, M. I. and Perel, V. I. 1965 Sov. Phys. JETP 20, 997; 21, 227.

Elbel, M., Kamke, B. and Schneider, W. B. 1974 Physica 77, 137.

Fano, U. 1957 Rev. Mod. Phys. 29, 74.

Gallagher, A. and Lewis, E. L. 1974 Phys. Rev. A 10, 231.

Guiry, J. and Krause, L. 1972 Phys. Rev. A 6, 273.

Guiry, J. and Krause, L. 1976 Phys. Rev. A 14, 2034.

Krause, L. 1975 in The Excited State in Chemical Physics, J. W. McGowan, Ed., John Wiley and Sons, Inc., New York.

Lewis, E. L., Wheeler, C. S. and Wilson, A. D. 1977 J. Phys. B 10, 2619.

Nesmeyanov, A. N. 1963, Vapour Pressure of the Elements, Academic Press, New York.

Millman, S. and Kusch, P. 1940 Phys. Rev. 58, 438.

Mitchell, A. C. G. and Zemansky, M. W. 1961, Resonance Radiation and Excited Atoms, Cambridge University Press.

Omont, A. 1965 J. Physique 26, 26.

Sieradzan, A. and Franz, F. A. 1982 Phys. Rev. A 25, 2985.

Skalinski, P. and Krause, L. 1982 Phys. Rev. A 26, 3338.

Skalinski, P. 1982 Ph.D. Thesis (University of Windsor) unpublished.

VITA AUCTORIS

I was born in Hamilton, Ontario on March 28, 1960. I attended primary school and J. L. Forster Secondary School in Windsor, Ontario, and upon graduation from high school in 1978 I enrolled at the University of Windsor. I graduated in 1982 with an Honours B.Sc. degree in Physics and I embarked upon graduate studies toward an M.Sc. degree.